UNIVERSITY OF CALIFORNIA
RIVERSIDE

Development of Novel Diagnostic Tools and beyond for Targets of Human Significance: Metabolites, Toxins & Viruses

A Dissertation submitted in partial satisfaction
of the requirements for the degree of

Doctor of Philosophy

in

Cell, Molecular and Developmental Biology

by

Lakshminarasamamba Cella

December 2012

Dissertation Committee:
Dr. Ashok Mulchandani, Co-Chairperson
Dr. Wilfred Chen, Co-Chairperson
Dr. Marylynn V. Yates

The Dissertation of Lakshminarasamamba Cella approved:

Committee Co-Chairperson

Committee Co-Chairperson

University of California, Riverside

Acknowledgements

I would like to thank my committee: Dr. Wilfred Chen, Dr. Ashok Mulchandani and Dr. Marylynn V. Yates, for their guidance and constant support. Due to their timely advice and efforts, I believe I have become a better researcher than I was when I started with the program. I would like dedicate my doctoral degree and all my achievements so far, small and big to my mother. She is responsible for making me a passionate, hardworking and dedicated individual that I am today and always encouraged me to follow my dreams. There is nothing in this world I could possible do to thank her. I would also like to thank my husband, whom I have known for just a few months but has shown enormous support and respect for my work and for all his endless love. I am thankful to the publishers of the journals for their permission to reprint the papers

1. Nano Aptasensor for Protective Antigen Toxin of Anthrax, Lakshmi N. Cella, Pablo Sanchez, Wenwan Zhong, Nosang V. Myung, Wilfred Chen, and Ashok Mulchandani, Analytical Chemistry 2010 82 (5), 2042-2047
2. Single-Walled Carbon Nanotube-Based Chemiresistive Affinity Biosensors for Small Molecules: Ultrasensitive Glucose Detection, Lakshmi N. Cella, Wilfred Chen, Nosang V. Myung, and Ashok Mulchandani, Journal of the American Chemical Society 2010 132 (14), 5024-5026

that appear in these journals and form a part of this dissertation.

ABSTRACT OF THE DISSERTATION

Development of Novel Diagnostic Tools and beyond for Targets of Human Significance: Metabolites, Toxins & Viruses

by

Lakshminarasamamba Cella

Doctor of Philosophy,
Graduate Program in Cell, Molecular and Developmental Biology,
University of California, Riverside, December 2012
Dr. Ashok Mulchandani, Co-Chairperson
Dr. Wilfred Chen, Co-Chairperson

Tools for the rapid assessment of diseased condition and underlying causative agent, disease progression and treatment outcome are prerequisites to meeting the goal of providing best health care possible. These tools should be highly selective and sensitive, show rapid response and of low cost for their wide spread use. Utilizing the growing knowledge about the organisms/conditions causing the diseased state, identifying suitable biomarkers and by incorporating newer technologies, novel diagnostics tools with above mentioned qualities can be built. Utilizing Single walled carbon nanotubes (SWNTs) we have built biosensors for detection of Protective antigen (PA) toxin secreted by anthrax causing bacteria and ultra-sensitive detection of glucose in unconventional body fluids. These nano-biosensors display high sensitivity and selectivity for the target can be easily adapted to develop point of care devices. Through these sensors we have

established a methodology for SWNT based sensor fabrication and shown different modes of operation for detection of both charged and uncharged analytes. Utilizing fluorescence based protein probe, we have developed an *in vivo* assay for HIV detection. This probe is sensitive to HIV protease, which is synthesized during its replication and plays an important role in formation of viable viral progeny. We are also able to assess the HIV protease activity in vivo against several wild type and mutant versions of its natural cleavage sites. These quantified kinetic parameters will help in gaining better understanding of protease-substrate and protease-inhibitor interactions. By mimicking the drug resistance causing protease and cleavage site mutations in our assay we can capture the altered kinetics and gain understanding of their contribution to resistance towards protease inhibitors. Our cell based assay is a better choice than the in vitro assay for screening newer inhibitors as it mimics the natural environment encountered by the enzyme and also provides the initial bioavailability and toxicity data for the candidate drugs.

Table of Contents

Chapter 1: **1**

Introduction **2**

Chapter 2 6

Abstract **7**

Introduction **8**

Material and Methods **11**

Results and Discussion **16**

Legends to Table **21**

Legends to Figures **22**

Chapter 3 ..... **29**

Abstract **30**

Introduction **31**

Materials and Methods **33**

Results and Discussion **35**

Legends to Figures **40**

Chapter 4 ..... **46**

Abstract **47**

Introduction **48**

Materials and Methods **54**

Results and Discussion **62**

Conclusion **68**

Legends to Table **69**

Legends to Figures **70**

Conclusion **85**

References **87**

Table of Figures

Figure 2. 1 Schematic illustration of aptasensor fabrication steps..... **24**

Figure 2. 2 Current versus voltage (I-V) curves of 1) unfunctionalized carboxylated SWNTs, 2) PASE modificated SWNTs, 3) aptamer immobilized SWNTs, and 4) after incubation with PA toxin **25**

Figure 2. 3 Calibration plot of the PA toxin sensor. Data is average of 6 independent sensors prepared at different times and error bars represent ±1 standard deviation. The inset is the magnification of sensors response at lower concentrations; r2 = 0.99 for the line..... **26**

Figure 2. 4 Specificity of the sensor without PA toxin aptamer (dark bars) and sensors with aptamers (striped bars) for different analytes. **27**

Figure 2. 5 Regeneration of the aptasensor upon treatment with 6M Guanidium chloride. Data is the average of 6 independent sensors prepared at different times and error bars represent ±1 standard deviation 28

Figure 3. 1 Schematic of displacement-based chemiresistive biosensor..... **41**

Figure 3. 2 I-V characteristics of the biosensor at various stages of fabrication and upon addition of glucose..... **42**

Figure 3. 3 Response of SWNTs modified with DexP and Tween20 minus the ConA to 1 nM glucose, 0.1 mM MnCl2 and 0.5 mM CaCl2 prepared in 10 mM phosphate buffer.. **43**

Figure 3. 4 Biosensor calibration for glucose in 10mM phosphate buffer (a) and in human plasma (b). Data points are average of four independent sensors (for each

investigation) prepared at different times and error bars represent ±1 standard deviation. **..... 44**

Figure 3. 5 Biosensor selectivity for various sugars (1 nM in 10mM phosphate buffer). Data points are average of 3 independent sensors prepared at different times and error bars represent ±1 standard deviation**..... 45**

Figure 4. 1 HIV life cycle. (A) Binding and entry, (B) uncoating, (C) Proviral DNA synthesis and transport into nucleus, (D) integration of the HIV proviral DNA into the host genome, (E) activation and synthesis of mRNA from proviral DNA and its transport into cytoplasm, (F) translation of the mRNA into gag and gag-pol polyproteins and release of protease from the gag polyprotein, (G) release of other viral proteins by action of the protease and their assembly into new virions and release (H)**. 72**

Figure 4. 2 HIV protease sensitive protein FRET module **..... 73**

Figure 4. 3 Fluroscence spectra obtained by conjugating varied protein (MACA-Alexa) molar concentrations with fixed Qdot concentration depicting the FRET **..... 74**

Figure 4. 4 FRET characterization. E – FRET Efficiency, r – actual separation distance, R0 – Forster distance. **..... 75**

Figure 4. 5 Temporal capture of the Qdot-MACA-alexa protein probe in vivo **..... 76**

Figure 4. 6 Capture of fluorescent changes with Qdot-MACA-alexa probe and nonspecific Qdot-WNV-alexa protein in both control and transfected wells**..... 77**

Figure 4. 7 A. The fluorescence images corresponding to the delivery of varying MACA-alexa protein to Qdot conjugated samples and B. the calibration plot correlating the fluorescence changes (FRET/Qdot) with in vivo probe concentration **..... 78**

Figure 4. 8 A. Quantified fluorescence changes of Qdot-MACA-alexa probe processing over time, B. Corresponding plot of quantified changes in intact probe concentration vs time, the slope of which gives the Vmax **..... 79**

Figure 4. 9 A. Temporal capture of fluorescence changes of Qdot-NCp1 WT- alexa probe in control and transfected samples, B. Plot of quantified changes in intact probe concentration vs time, the slope of which gives the Vmax **..... 80**

Figure 4. 10 A. The sequence of the mutant NC-p1 site as opposed to the wild type, B. Temporal capture of the fluorescent changes of Qdot- NCP1 M2-alexa protein in control and transfected samples, C. Plot of quantified changes in intact probe concentration vs time, the slope of which gives the Vmax **..... 81**

Figure 4. 11 A. Amino acid residues of Wild type HIV-1 (HXB2) protease (above the bar) with their location (numbers within the bar) and the mutated residue (below the bar). The highlighted amino acid at where mutated by site-directed mutagenesis, B. The combined plot of changes in Qdot-MACA-alexa probe concentration in vivo with time in case of wild type protease (HXB2) and mutant HIV protease (V82A and L90M). **..... 82**

Figure 4. 12 A. Inhibition efficiency of indinavir in case of wild type (HXB2) protease and mutant (V82A) protease, B. Inhibition efficiency of saquinavir in case of wild type (HXB2)

protease and mutant (L90M) protease, C. Tabulated values of reported and estimated IC50 values for mutation and inhibitor combinations..... **83**

List of Tables

Table 2. 1 Sequences of Clones obtained from ssDNA pool after six round of selection and CLUSTAL W (1.83) multiple sequence alignment **…….. 36**

Table 4. 1 Tabulated values of reported and estimated IC50, for mentioned mutation and inhibitor combination .**……98**

Chapter 1:

Introduction

Introduction

In order to provide the best possible treatment to a patient ensuring survival, there is a need for identifying the underlying condition early/sensitively, with specificity and preferably in a non-invasive fashion. These technologies have to be affordable so that a huge population can benefit from them. Numerous efforts have been made to address these issues using newer technologies and develop novel diagnostic technologies. Some of the major health concerns worldwide include diabetes, cancer, cardiovascular diseases, pathogens used as bioweapons, viruses. The identification of biomarkers for several of these conditions and understanding of the pathogenicity of the infectious organism has led to development of efficient strategies for their detection and in some cases to develop treatment strategies. We have used some current technologies to build biosensor for detection of toxins released by pathogenic organisms, biosensor for highly sensitive glucose detection and developed an assay for human immuno deficiency virus (HIV) detection and for screening of anti-HIV drugs.

Among the different technologies employed, nanotechnology has been very popular for building biosensors. In case of nano-biosensors, the traditional transducer element (element converting biological event into measurable quantity) is replaced with a one dimensional (1-D) nanomaterial. These nanomaterials provide advantage of high sensitivity and selectivity, point of care devices of low-cost can be built for rapid

detection. Multiplexed devices can be built using nanomaterials for detection of a number of analytes at the same time.

We have built nano-biosensors using single –walled carbon nanotubes (SWNT) capable of detecting the anthrax toxin and glucose. SWNTs are a widely sought after 1-D nanomaterial owing to their excellent electrical properties, high surface to volume ratio and for having an active surface that is sensitive to any adsorption/electronic events [1], [2]. Numerous SWNT based biosensors have been built for variety of targets [2–8] and utilizing different bio-recognition elements. Anthrax is caused by bacteria *Bacillus anthracis* through a toxin it makes. Infection by anthrax causing bacteria is hard to detect early on due to nonspecific symptoms and results in high mortality. The toxin is a three component system with protective antigen (PA) toxin being one central part. PA toxin has been found earlier to be an effective target for controlling the infection [9]. We have selected a DNA aptamer against the PA toxin and immobilized it onto the SWNTs to build a biosensor for anthrax detection. Aptamers are oligonucleotides capable of binding a target molecule with high affinity and specificity. Upon immobilization of PA toxin aptamer on SWNT surface and the binding of PA toxin to the aptamer results in change in the conductance of the SWNT channel. This change is recorded and can be correlated to PA toxin concentration in the sample. This aptamer based sensor displays excellent selectivity and high sensitivity, both of which are very crucial for early detection of this infection to ensure the survival of the infected. The

same SWNT platform was adapted with different bio-recognition element for detection of very low levels of glucose, a major metabolite. Several applications involve detection of glucose at extremely low levels, like in case of tears, saliva and urine [10–12]. Since glucose is not charged, the detection mechanism similar to PA toxin sensor would not be applicable as there would not be sufficient conduction variations in the SWNT channel. Thus we chose to use a displacement mode of assay, wherein a more charged molecule is immobilized onto the SWNT surface and presence of glucose in the sample would displace it and change the conductance across the SWNT channel. We immobilized concavalin A (Con A), a plant lectin through dextran onto SWNTs. Upon introducing glucose, it would bind to ConA and displace it off the surface and the resulting conductance changes are proportional to the glucose concentration.

HIV is the causative organism of acquired immune deficiency syndrome (AIDS), one of the major epidemics worldwide. The nature of this virus to continuously evolve has made it impossible to develop definitive treatment strategies or preventive vaccines. However the increasing knowledge about its structure, life cycle and pathogenicity has led to development of very efficient diagnostic technologies and effective drugs. HIV protease inhibitors are a major class of drugs employed in anti-HIV therapy and shown to be successful in blocking the infection. This enzyme plays a central role in the life cycle of the virus and blocking its function would lead to production of non-infectious viral particle. We have built a fluorescence based probe that is sensitive to HIV protease

and developed a cell based assay that can detect as well as capture the activity of the protease. This enzyme, like the rest of virus evolves by accumulating mutations and over a period of time becoming resistant to the drugs currently available. Thus there is a need for better protease inhibitors that can provide a high barrier for resistance development. Our assay forms an excellent choice for identifying new inhibitors against the protease. This assay has several advantages over other drug screening methodologies as it is a cell based providing more natural environment for the protease, mutations within protease can be mimicked to identify better inhibitors and also they provide the initial estimate of the toxicity of the potential candidates.

In the following chapters, a more comprehensive rational for our targets chosen and technologies used is provided along with the experimental details and results.

Chapter 2:

Nano aptasensor for protective antigen toxin of anthrax

Abstract

We demonstrate a highly sensitive nano aptasensor for anthrax toxin through the detection of its polypeptide entity, protective antigen (PA toxin) using a PA toxin ssDNA aptamer functionalized single-walled carbon nanotubes (SWNTs) device. The aptamer was developed in-house by capillary electrophoresis systematic evolution of ligands by exponential enrichment (CE-SELEX) and had a dissociation constant (K_d) of 112 nM. The aptasensor displayed a wide dynamic range spanning up to 800 nM with a detection limit of 1nM. The sensitivity was 0.11 per nM and it was reusable six times. The aptasensor was also highly selective for PA toxin with no interference from human and bovine serum albumin, demonstrating it as a potential tool for rapid and point-of-care diagnosis for anthrax.

Introduction

Anthrax is a disease caused by the anthrax toxin of the spore forming Gram positive bacterium *Bacillus anthracis*. Many of the properties of *Bacillus anthracis* such as high mortality and environmental stability make them a deadly bioterrorist agent that can used by terrorist organizations to cause wide spread casualties. The early stage of anthrax infection is often characterized by non-specific symptoms making its detection difficult. Therefore, there is a great need for prompt administration of antibiotics before a lethal infection is established. This is particularly relevant for the inhalational form of the disease. In fact, of the five fatalities in the 2001 bioterrorist attacks in the United States involving anthrax, infection was confirmed in only one individual before death [13].

The pathogenecity of the anthrax bacteria is mainly due to the tripartite toxin it makes. The three components of the toxin are cell-binding protective antigen (PA), edema factor (EF) and lethal factor (LF). Assembly of the three toxin proteins is initiated when PA binds to a cellular receptor[14] and is activated by cleaving PA into two fragments: PA20 (20 kDa), PA63 (63 kDa). Receptor-bound PA63 then spontaneously self-associates to form ring-shaped, heptameric oligomers [15]. EF and LF bind competitively to PA63 subunits [16], and are translocated across the membrane to the cytosol. Once within the cytosol, EF catalyzes the conversion of ATP to cAMP [17], and LF proteolytically cleaves certain MAP kinases [18] thus disrupting the normal functions

of the cell and manifesting the disease. The protective antigen is thus an essential factor and plays an important role in the immune response. It has been demonstrated that antibodies against the PA toxin possess a neutralizing effect of the toxin as well as anti-spore activities [9], making the PA toxin an ideal target for detection of the infection. Current detection methods involving cell culture, immunological tools, electrophysical measurements of ion channels [19] and nucleic acids while effective are not suitable for early detection [20]. Therefore, a rapid, facile, sensitive and selective method of detecting anthrax toxin in body fluids would provide an invaluable tool for establishing whether anthrax is the causative agent of a biological attack leading to prompt diagnosis and targeted treatment of infected individuals.

Single-walled carbon nanotubes (SWNTs) have been extensively studied as the transducer elements of biosensors as they meet the important requirements of an efficient biosensor: excellent electrical properties and a large surface to volume ratio results in surface phenomena predominating over the chemistry and physics that happen in the bulk [1], [2]. These along with suitable bioreceptors have shown to make sensors that display high selectivity, sensitivity and real-time label-free detection capabilities. SWNTs have been successfully used to detect a variety of targets [21–28]. Proteins (enzymes, antibodies) and more recently aptamers [3–7] are the commonly used probes to detect the target analytes. Detection of anthrax infection at high sensitivity using other nanomaterials: europium nano materials has been reported earlier and it further proves their efficiency as transducers in biosensors [29], [30].

Aptamers are short, synthetic oligonucleotides capable of binding to wide variety of molecules with high affinity and specificity. Aptamers as probes are more advantageous compared to antibodies as 1) their synthesis does not require animal host or expensive hybridoma culture, 2) can be selected using modern combinatorial chemistry tools and 3) are more stable. For example, systematic evolution of ligands by exponential enrichment (SELEX) is the technique used to identify DNA or RNA aptamers with high affinity and specificity for different targets [31], [32]. SELEX employs a random library of oligonucleotides from which sequences with desired characteristics of affinity and specificity are selected. A number of different SELEX processes have been proposed since its inception based on the differences in the techniques used to separate the bound and unbound random library. Capillary electrophoresis-SELEX (CE-SELEX), a variant of the conventional SELEX, uses a solution based binding and separation technique to alleviate the drawbacks of selection bias encountered in the conventional SELEX. The technique has been applied to different targets - Human IgE, HIV-1 Reverse Transcriptase, neuropeptide *Y* [33], [34].

Here we report the development, characterization and evaluation of a highly sensitive and selective aptasensor for the detection polypeptide entity PA of anthrax toxin in plasma. The aptasensor consisted of ssDNA aptamers for the PA63 selected in-house using CE-SELEX from a DNA library integrated to a SWNTs-based chemiresistive transducer.

Material and Methods

Materials

The DNA library and Primers for PCR were acquired from Integrated DNA Technologies Inc. (Coraville, IA, USA). Streptavidin Agarose beads for single strand regeneration were obtained from Pierce (Rockford, IL, USA). Bare fused silica capillary (40 cm long by 50 µm I.D. and 360 µm O.D.) coated with polyvinyl alcohol was obtained from Polymicro Technologies (Phoenix, AZ, USA). PA toxin was purchased from List Biological Laboratories, Inc. (Campbell, CA, USA). Taq Polymerase and pGEM vector were purchased from Promega Corp. (Madison, WI, USA). CE – SELEX was performed in P/ACE MDQ Capillary Electrophoresis system (Beckman Coulter, Inc., Fullerton, CA, USA). Selection Buffer consisted of 25mM Tris, 10 mM NaCl and 1 mM $MgCl_2$, bead binding/washing buffer was 100 mM phosphate buffer and 50 mM NaCl. Single-walled carbon nanotubes with high carboxylated functionality, sold under the trade name of P3-SWNT, were purchased from Carbon Solutions, Inc. (Riverside, CA, USA). Human serum albumin and bovine serum albumin were purchased from Sigma-Aldrich (Milwaukee, WI, USA). 1-pyrenebutanoic acid succinimidyl ester (PASE) was purchased from Invitrogen (Carlsbad, CA, USA).

Methods

Aptamer Generation:

Capillary electrophoresis selection: The synthetic DNA library of 40 random nucleotides flanked by 20 bases priming sites for PCR amplification in selection buffer was heated to 94^{o}C and cooled to room temperature followed by incubation with 20 nM of PA toxin for 20 min at room temperature. Approximately 150 nL of the above mixture was injected into the conditioned (washing/rinsing with 150 nL each of 100 mM HCl, 100 mM NaOH, double distilled H_2O and selection buffer) bare fused silica capillary of a P/ACE MDQ Capillary Electrophoresis system using 2.5 psi pressure for 13 s. An electric field of 30 kV was applied to enable the migration using normal polarity at a temperature of 25 °C and the separation of PA toxin-DNA complex and unbound DNA was monitored using a UV detector at 254 nm. All sequences migrating more than 30 s earlier than the leading edge of the peak corresponding to the unbound sequences were collected into 20 μl of separation buffer at the capillary outlet. The exact time that the unbound sequences would reach the outlet of the capillary was calculated from the knowledge of the distance from the end of the capillary to the detector and experimentally determined migration time for the naïve library.

PCR amplification: The 20 μl of the collected fraction containing the bound sequences were divided into four aliquots. PCR buffer was added to these fractions so that the final reaction mixture contained 1 mM of each deoxyribonucleotide triphosphate (dNTP), 1 μM of primer 1 (5'-AGC AGC GAG GTC AGA TG-3'), 1 μM of primer 2 (biotin/5'-TTC ACG

GTA GCA CGC ATA-3'), 0.15 U/μl of Taq polymerase, 7.5 mM $MgCl_2$, 1 mM PCR buffer and 5μl of the collected fraction as template. PCR was carried out by heating the mixture to 95 ^{o}C for 5 min followed by 11 cycles of denaturation, annealing and extension for 30 s at 95 ^{o}C, 53 ^{o}C for 30 s and 72 ^{o}C for 20 s, respectively. Control PCR without any added DNA was also performed. The presence of DNA following PCR was confirmed by electrophoresis on a 2% agarose gel followed by staining with ethidium bromide.

The PCR amplified product was conjugated to streptavidin coated agarose beads, washed with binding buffer and then melted by treatment with 200μl 0.15M NaOH. The single stranded DNA was then concentrated using QIAEX II DNA Extraction Kit Qiagen (German Town MA).

Cloning: A PCR amplified product was ligated to pGEM vector transformed into DHα5 *E. coli* using electroporation. Colonies were grown on LB-agar medium supplemented with ampicilin and X-Gal and IPTG. Transformed colonies were selected and sequenced at the University of California, Riverside Genomics Institute, Riverside, CA. The dissociation constants (Kd) for selected clones was determined by Affinity Capillary Electrophoresis (ACE) performed under the same conditions as CE-SELEX. In the ACE process the aptamers were initially labeled with a 6-carboxyfluorescein and incubated with increasing concentration of PA Toxin. The peak heights of the unbound DNA was used to

calculate the Kd values. Nonlinear least-squares regression analysis was performed to determine the Kd using GraphPad Prism 4 (GraphPad Software, San Diego, CA USA).

Biosensor Fabrication:

Solubilizing SWNTs and alignment*:*

Carboxylated-SWNTs (SWNT-COOH 80-90% purity) (Carbon Solution, Inc. Riverside, CA, USA) were dispersed (1 μg/mL) in dimethyl formamide (DMF, Sigma Aldrich, MO, USA) using ultrasonic force for 60 min followed by centrifugation (10,000 RPM) to remove unsolublized SWNTs. These processes were repeated three times with decreasing time 90, 60, and 30 min to prepare soluble SWNTs. The suspended SWNTs were aligned in the 3 micron spaced microfabricated gold electrodes by AC dielectrophoresis (DEP). In brief the procedure involves addition of 0.1 μl drop of SWNTs and applying AC voltage at a frequency of 4MHz (amplitude 0.366 V p-p) across the electrodes. The aligned SWNTs are then annealed at 300 °C for 60 minutes under reducing atmosphere (5% H_2 + 95% N_2) to minimize the contact resistance between the CNT network and the gold electrodes and to remove any DMF residues. The number of SWNTs bridging the electrode gap was controlled by adjusting the concentration of the SWNTs in the DMF solution and the droplet size.

Aptamer functionalization of SWNTs: The SWNTs are noncovalently modified using 6 mM 1-pyrenebutanoic acid, succinimidyl ester by technique developed by Chen et

al.[22] In brief, the process involved incubating the sensor (with annealed SWNTs) with 6 mM 1-pyrenebutanoic acid, succinimidyl ester in DMF for one hour followed by thorough washing with DMF to remove excess chemical. The sensor was then rinsed with phosphate buffer (10 mM) and nanopure water. The apt 11(PA toxin aptamer) was attached onto the SWNTs by incubating with 5µM aptamer solution in 10 mM phosphate buffer overnight at 25^0C, followed by treatment with 0.1 mM ethanolamine to block excessive reactive groups for 30 min [35], and finally by incubation with 0.1 % Tween 20 to prevent non-specific binding.

Sensing measurement: The devices were incubated with 5 µl of the sample for 1 min, washing the device 3 times with 10 mM phosphate buffer, 1 times with nanopure water followed by aspirating the water and measuring the I-V response in ambient air using a Keithley Source Meter (Model 236).

Results and Discussion

PA toxin aptamer selection: Because of the well documented central role of PA toxin, the B component of the A-B type anthrax toxin [36], in manifestation of the disease, a number of immunoassays/sensors utilizing the high affinity antibodies single chain antibody fragments and affinity peptide against PA toxin have been developed [19], [37–39]. However, due to antibodies potential instability from proteolysis and the need of animal host or expensive hybridoma culture to produce, we chose to work with aptamers that are characterized by their higher stability, easy regeneration upon binding to an analyte, inexpensive *in vitro* synthesis and similar high affinity as antibodies. Previously, an RNA aptamer against PA toxin was generated by Archemix Corporation, Cambridge, MA, USA, under an U.S. Army Research Office contract [40]. Since DNA sequences, with and without terminal modifications, are more resistant to nucleases than RNA sequences [41], we chose to work with DNA aptamers. Aptamer for PA toxin was selected from a synthetic library of single stranded DNA (ssDNA) using CE-SELEX. Based on the initially established migration pattern of the library with or without PA toxin (data not shown), PA toxin-library complex was collected separately from the unbound library and PCR amplified (eleven cycles). The purified ssDNA from the PCR products was incubated with the PA toxin for the next round of SELEX. After 6 rounds of selection, the selected library was cloned and 9 clones were selected for further analysis and sequencing. As shown in Table 1, sequenced clones resulted in no consistent

homology when analyzed with ClustalW, which was consistent with published results [42]. The dissociation constant (K_d), determined by affinity capillary electrophoresis (ACE), ranged from 112 - 1140 nM. The K_d of 112 nM for the best aptamer (Apt11) was ~4-fold better compared to the PA toxin RNA aptamer (400 nM) [40] and in line with the K_d of other reported high affinity DNA aptamers.

SWNTs-based PA toxin aptasensor: The Apt11 PA toxin specific aptamer generated above was applied for development of the PA toxin nano aptasensor. Carboxylated SWNTs were used in our experiments to get a uniform suspension of well-separated SWNTs prior to AC dielectrophoretic alignment between microfabricated gold electrodes. Since the first use of alternating current to position carbon nanotubes [43] the process has been used extensively to align SWNTs across micro spaced electrodes. The major advantage of this technique is that it provides better control in positioning and contacting the SWNTs between metal electrodes for electronic circuits compared to the techniques of drop-casting, spray-coating and catalytic growth at high temperatures or self-assembly. Alignment of the SWNTs was performed at $0.3V_{P-P}$ and 4 MHz frequency for 5s as these parameters reproducibly gave a uniform distribution of well contacted SWNTs across the electrodes as observed under SEM and an initial resistance in the range of 20-100 KΩ after annealing at 300 ^{o}C for 1 h under 5% H_2 and 95% N_2 environment. Fig.2.1 shows the schematic of the steps involved in the functionalization of SWNTs with aptamers. In order to preserve the aptamer activity, the immobilization onto the SWNTs was accomplished using 1-pyrenebutanoic acid succinimidyl ester

(PASE) [22]. PASE non-covalently attaches to the SWNTs through the highly aromatic pyrenyl group by pi-pi bond interaction and provides a free succinimidyl ester group that can interact with the amine group at the 5' end of the PA toxin aptamer by the formation of an amide bond. The non-covalent modification of the SWNTs helps to protect their electronic properties and also provides high degree of control and specificity for immobilizing biological molecules. Immobilization of aptamers was followed by incubation with 0.1 M ethanolamine for 30 min [35] to neutralize/passivate excess free succinimidyl ester reactive groups and finally with 0.1% Tween20 for 30 min to block non-specific protein adsorption (NSPA) on SWNTs [22].

The high surface area to volume ratio and the surface carbon atoms make SWNTs extremely sensitive to perturbations/adsorption events at the surface. This was also evidenced in the present study as illustrated by the modulation of the current vs. voltage (I-V) characteristics after each event (Fig. 2.2). In accordance with the literature reports, aptamer immobilization onto the SWNTs decreased the device resistance (trace 3, Fig. 2.2) compared to the PASE-functionalized SWNTs (trace 2, Fig. 2.2) owing to the accumulation of negative charges from the phosphate backbone of ssDNA aptamers [5], [43]. The incubation of the aptamer-functionalized SWNTs device with 1 μM of target analyte (PA toxin) for 1 min at room temperature dramatically increased the device resistance (trace 4, Fig. 2.2), attributed to positive charge accumulation of the PA toxin bound to the aptamer. The later demonstrated the potential for electrical detection of PA toxin using a simple SWNTs-based chemiresistive aptasensor.

Fig. 2.3 shows the relationship between the SWNTs based chemiresistive aptasensor response [$(R - R_0)/R_0$, where R is the resistance after exposure to PA toxin and R_0 is resistance after exposure to buffer] and PA toxin concentration. The resistance is calculated as the inverse of the slope of the I-V plot between -0.1 and +0.1 V (linear range). The dissociation constant of the PA toxin aptamer calculated from the aptasensor calibration was determined to be 225 nM. This is slightly higher than the 112 nM determined from ACE and can be explained by the fact that the aptamer is immobilized in the case of aptasensor as opposed to in the solution phase in ACE study. The aptasensor was highly sensitive, 0.11 per nM in the linear region, with a limit of detection of 1 nM. Furthermore, it had a wide dynamic range spanning up to 800 nM with a linear dynamic range up to 400 nM. The limit of detection of our aptasensor while higher than the 16 pM reported for a sandwich ELISA, the sensing required only 1 min incubation and a single recognition molecule (aptamer) as opposed to two recognition molecules, a capture single chain antibody and a secondary IgG, one hour incubation each with the capture and secondary antibodies and signal amplification through the biocatalyst horseradish peroxidase label [44].

Selectivity/specificity is a critical parameter in the acceptance/utility of a sensor. The aptasensor had excellent selectivity as evidenced by an insignificant response to both Human serum albumin (dominant protein in human blood) and Bovine serum albumin (dominant protein in bovine blood) when compared to PA toxin (Fig. 2.4). Additionally,

negative controls, i.e. SWNTs devices without PA toxin aptamer show a very small response to PA toxin, HSA and BSA.

The potential of reusing a sensor several times either with or without a regeneration step is highly desirable. We investigated regenerating the aptamer so that the sensor can be used multiple times. Incubation of the aptasensor after use with 1 μl of 6 M guanidium hydrochloride for 15 min followed by through washing with 10 mM phosphate buffer restored its functionality for up to six repeated measurements (Fig. 2.5).

In conclusion, we synthesized ssDNA aptamers with good affinity (K_d = 112 nM) and selectivity for PA toxin by six rounds of CE-SELEX. Combining the aptamers with SWNTs transducer, an aptasensor for facile and rapid PA toxin detection was constructed. The 1 nM limit of detection, a wide dynamic linear range, high sensitivity and excellent selectivity make the sensor useful for direct detection in biological samples. The aptasensor also gives commercial advantage due to its simple fabrication scheme, small size and reusability. The performance of the sensor can be further improved by operating as a field-effect transistor, reducing the contamination of metallic nanotubes in the SWNT suspension and using an aptamer with lower K_d.

Legends to Table

Table 2. 1: Sequences of Clones obtained from ssDNA pool after six rounds of selection and CLUSTAL W (1.83) multiple sequence alignment

Legends to Figures

Figure 2. 1. Schematic illustration of aptasensor fabrication steps.

Figure 2. 2. Current versus voltage (I-V) curves of 1) unfunctionalized carboxylated SWNTs, 2) PASE modificated SWNTs, 3) aptamer immobilized SWNTs, and 4) after incubation with PA toxin.

Figure 2. 3. Calibration plot of the PA toxin sensor. Data is average of 6 independent sensors prepared at different times and error bars represent ±1 standard deviation. The inset is the magnification of sensors response at lower concentrations; r2 = 0.99 for the line.

Figure 2. 4. Specificity of the sensor without PA toxin aptamer (dark bars) and sensors with aptamers (striped bars) for different analytes. Analyte concentration is fixed at 100 nM and the incubation time was 1 minute. Data is the average of three independent sensors prepared at different times and error bars represent ±1 standard deviation.

Figure 2. 5. Regeneration of the aptasensor upon treatment with 6M Guanidium chloride. Data is the average of 6 independent sensors prepared at different times and error bars represent ±1 standard deviation.

Table 2. 1

clone	sequence	K_d (nM)
C1-PA-5	TCAGACACTTTGCCAAAAAACATGATACAAGTTCGCTGCC—40	173
C1-PA-10	—GCTTTACCGCACTTCCGATCTTTAATTTCGAGTGTATCAT—40	488
C1-PA-12	—CATCTCGGTCGTGAACTTTACATGCATGAGTATTTTGGTG—40	508
C1-PA-11	ATCACTAGTGAATTCGCG-GCCGCCTGCAGGTCGACCATAT—40	112
C1-PA-7	—CCCAACATCTACGGTTAGACCGGGTTTACCTGAGCTGACA—40	526
C1-PA-6	—TTTCTAGGAAATTCAAACAGGTTTGTATTTTTTCTAGTTGA—40	345
C1-PA-1	—CTATAGAGGTGCTCCAGGGCGATAAACTTATGAATATTAA—40	1140
C1-PA-3	—AGCTTAGTGCATATCACTCCTCGTTATAGCATGGTTATAG—40	661
C1-PA-9	—AAATGATTGCTACAATACATAGAGTCATGGAGATTACATC—40	509

Figure 2. 1

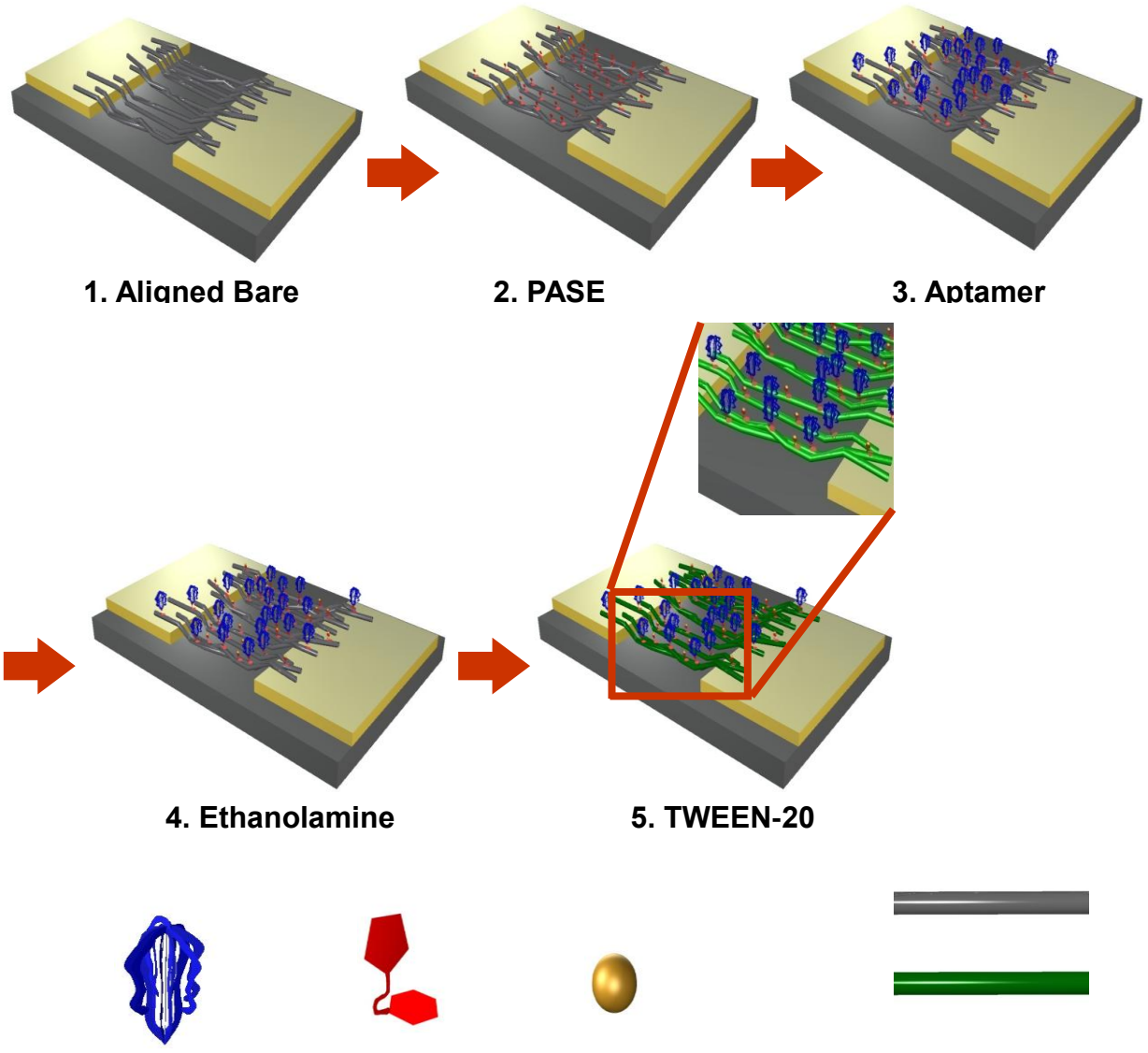

Figure 2. 2

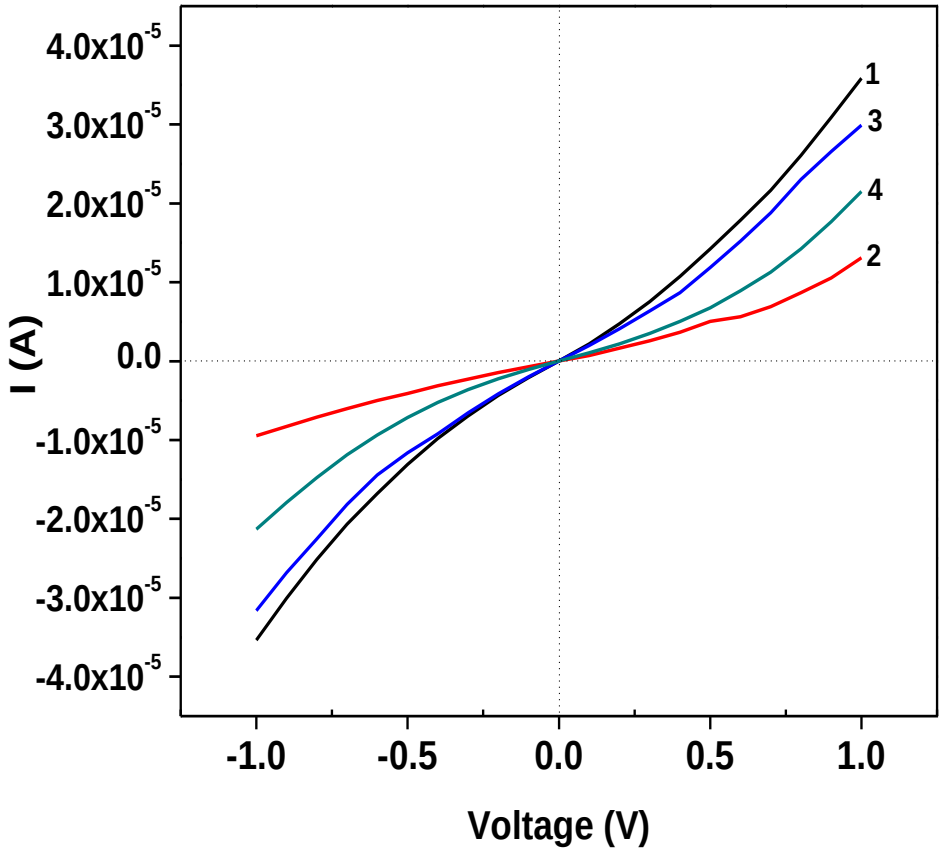
4.0x10-5
3.0x10-5
2.0x10-5
1.0x10-5
0.0
-1.0x10-5
-2.0x10-5
-3.0x10-5
-4.0x10-5
I (A)
-1.0
-0.5
0.0
0.5
1.0
Voltage (V)
1
3
4
2

Figure 2. 3

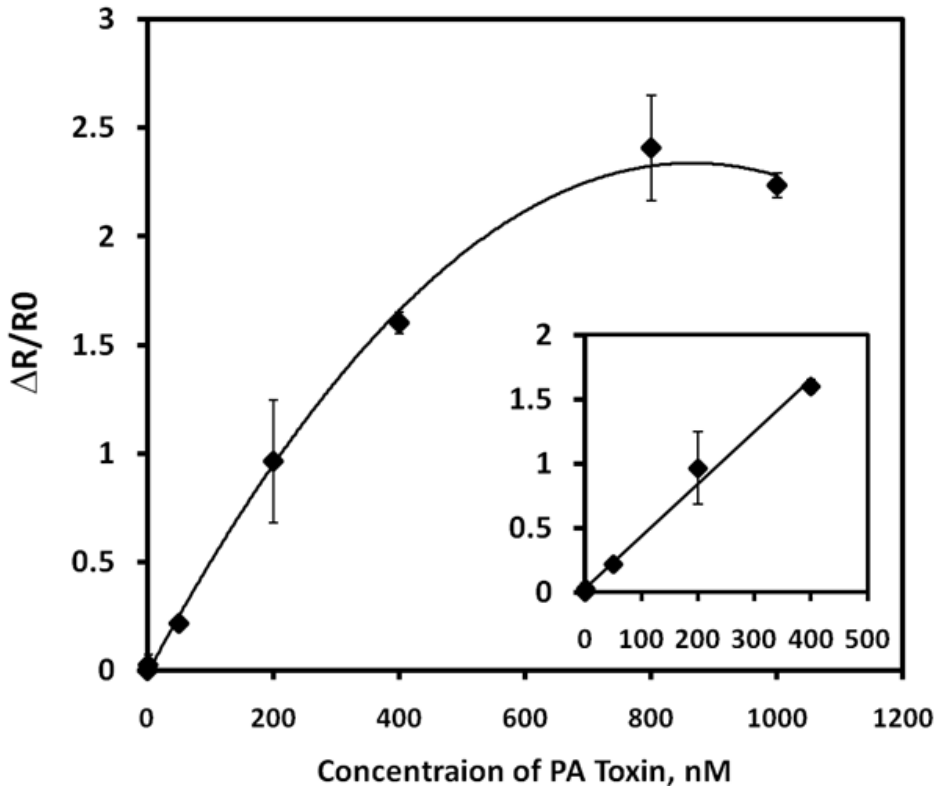
3
2.5
2
1.5
1
0.5
0
ΔR/R0
0
200
400
600
800
1000
1200
Concentraion of PA Toxin, nM
2
1.5
1
0.5
0
0
100
200
300
400
500

Figure 2. 4

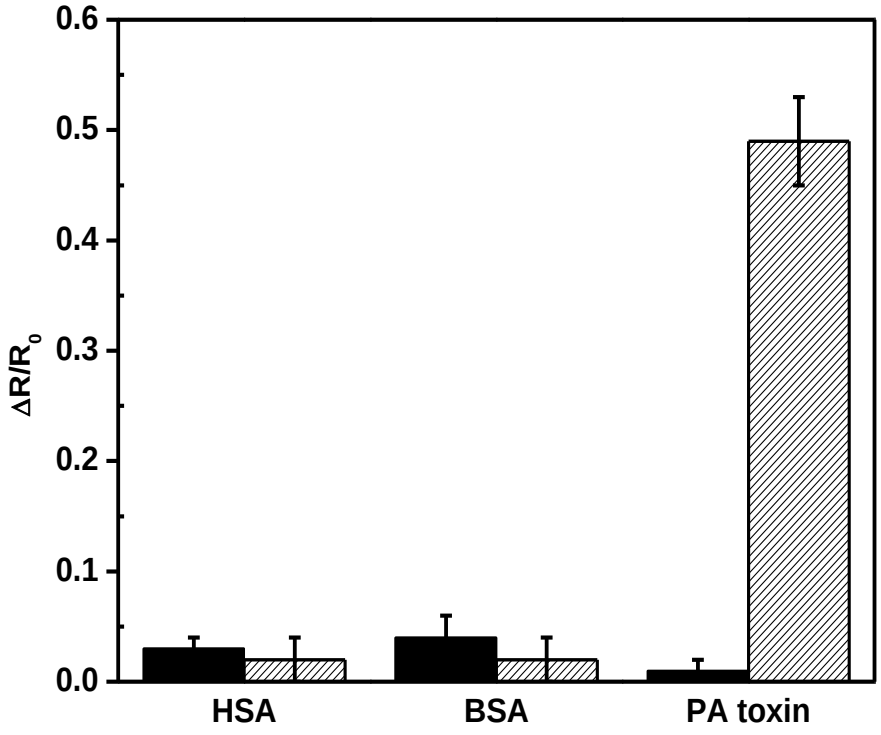

Figure 2. 5

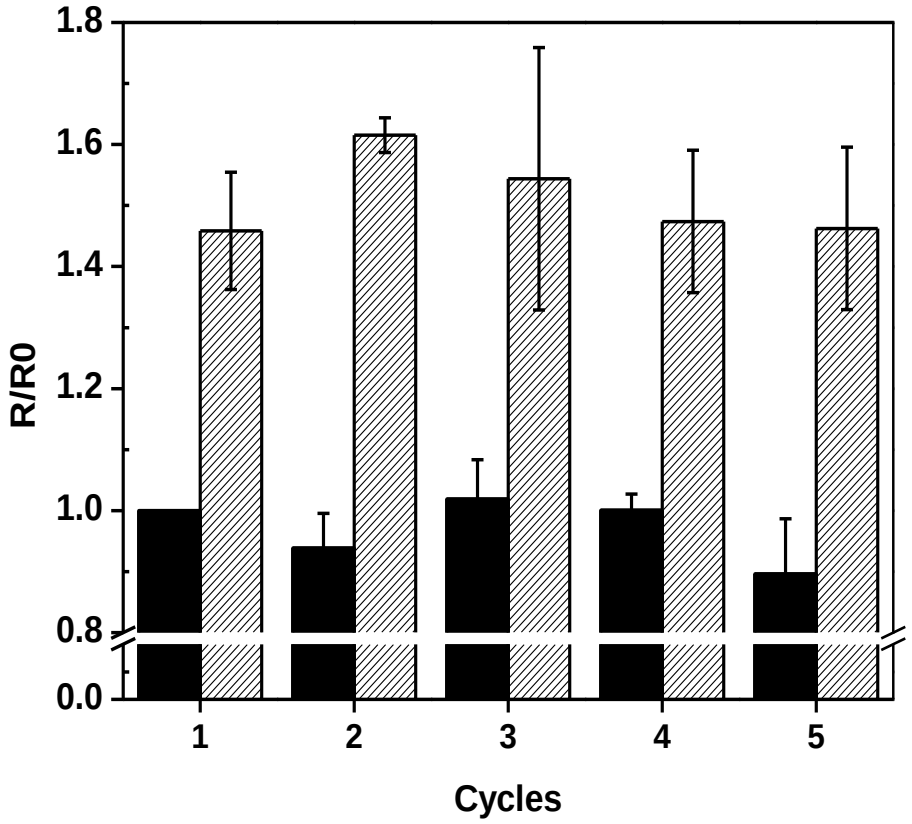

Chapter 3:

Single-Walled Carbon Nanotubes-Based Chemiresistive Affinity Biosensors for Small Molecules: Ultrasensitive Glucose Detection

Abstract

We report for the first time single wall carbon nanotubes (SWNTs)-based chemiresistive affinity sensors for highly sensitive and selective detection of small and/or weak-/un-charged molecules using displacement format. The detection of glucose, a small weakly charged molecule, by displacement of plant lectin, Concavalin A, bound to polysaccharide, dextran, immobilized on SWNTs, with picomolar sensitivity and selectivity over other sugars and human serum proteins is demonstrated as a proof-of-concept.

Introduction

In recent years, there has been an increasing interest on use of one-dimensional (1-D) nanostructures, such as nanowires, nanobelts and nanotubes, as transducer elements in affinity (bio)sensors. Use of nanomaterials provide high sensitivity with low limit of detection and in conjunction with molecular recognition element, high selectivity, for label-free, rapid and low-cost, multiplexed and point-of-care/field detection of various analytes. Single-walled carbon nanotubes (SWNTs) are one such class of nanomaterials that have been used extensively as sensing elements due to their excellent electrical properties, ultra-high surface area to volume ratio and surface atoms which are extremely sensitive to any surface adsorption/reaction events. SWNTs modified with biorecognition molecules such as antibodies, aptamers or DNA have been successfully used to detect various targets ranging from proteins [7], [22], [27], [45–47], viruses [48], bacteria [49], yeast [50], DNA/RNA [51–53] and even mammalian cancer cells [54]. Majority of these SWNT-based biosensors are affinity sensors wherein the binding of the analyte, generally a large charged antigen, to the bioreceptor immobilized on the surface of SWNTs leads to change in conductance of SWNTs channel.

Small, charged or uncharged, molecules constitute a large group of analytes of interest in the fields of environmental monitoring and health care. The detection of these analytes using SWNTs-based chemiresistive/field-effect transistor sensors using the traditional modes of affinity-based sensing might be ineffective as their binding to the

recognition molecule might not generate measurable change in conductance/resistance. Nanobiosensors that can detect and quantify such small molecules with high sensitivity and selectivity are therefore in urgent need. In an effort to achieve these objectives, we have for the first time employed the displacement immuno-assay/sensor format [55–60] on a SWNTs-based chemiresistive platform and demonstrated its effectiveness. In the displacement mode of operation, the SWNTs are initially functionalized with an analog of the target analyte having lower binding affinity to the biological recognition molecule than the actual analyte followed by binding to the biological recognition element such as antibody. Upon addition of the sample analyte to the device it competes with the analog for the bioreceptor and displaces it off the SWNTs channel leading to a change in the sensor conductance.

Materials and Methods

Materials:

Single wall carbon nanotubes (P3-SWNTs) were purchased from Carbon Solutions Inc (Riverside,

CA, USA). Dimethyl formamide (DMF), Tween 20, dextran (MW 70,000), 1,2–epoxy-3-phenoxypropane, Concanavalin A (ConA), glucose and human plasma were obtained from Sigma Aldrich (St. Loius, MO, USA). Phenoxy dextran (DexP) was synthesized using previously reported protocol [23]. In brief, 4 g of dextran was dissolved in 32 mL 1 N NaOH at 400C under constant stirring. After 24 h the product was flocculated with ethanol and collected by vacuum filtration. The flocculated product is then dissolved in nanopure water and dialyzed against the same for 24 h to remove any impurities. The purified product after measuring the absorbance at 269 nm to determine phenoxy content is then lyophilized.

SWNT suspension

A uniform suspension of SWNTs in DMF (10 µg/ml) was prepared by subjecting the mixture to

repeated cycles of sonication (power level 9) and centrifugation (10,000) with decreasing time

for each cycle (90, 60, 30 min).

Instrumentation:

The conductivity/resistance was measured at room temperature and in ambient air from the I-V

plots obtained using a semiconductor parameter analyzer (HP 4155A Hewlett Packard). The VWR sonicator at the highest power level and Beckman centrifuge were used for SWNTs suspension preparation. Wavetek function generator was the AC voltage source for SWNT alignment.

Results and Discussion

Figure 3.1 shows the schematic of the displacement-based chemiresistive affinity (bio)sensor. The principle behind the displacement mode based sensors is similar to the competitive mode of immunoassay. The well-characterized glucose-Concavalin A-dextran system [61–63] was evaluated as a model system to demonstrate displacement based chemiresistive mode of sensing. Concanvalin A (ConA), a plant lectin that binds non-covalently to some carbohydrates, is a metalloprotein with four carbohydrate binding pockets and can exist as a dimeric form at low pH or tetrameric form at neutral pH9. Polysaccharide dextran and monosaccharide glucose are among the carbohydrates that reversibly bind to ConA, with glucose displaying higher binding affinity which means that upon introduction of glucose to ConA-dextran complex, glucose displaces dextran from ConA (Figure 3.1). The binding of the ConA to carbohydrates results in changes to its conformation and alters its isoelectric point to far from neutral pH leading to accumulation of positive charge [64]. On the other hand, both glucose and dextran are electrically neutral over a wide pH range in free form as well as in the bound state to ConA. Thus, using this system in the chemiresistive configuration it's the binding and removal of ConA from the SWNTs that will result in conductance change due to its positive charge.

The process starts with preparation of AC dielectrophoretically aligned SWNT across a pair of 3 μm spaced microfabricated gold electrodes. In brief, the procedure involved

addition of 0.1 µl drop of SWNTs suspended in dimethyl formamide and applying AC voltage at a frequency of 4 MHz (amplitude 0.3 V peak to peak) across the electrodes. The aligned SWNTs were then annealed in place by heating at 3000C for an hour under inert environment maintained by continuously flowing nitrogen gas containing 5% hydrogen. This was followed by modification with dextran by overnight incubation at room temperature with 1 wt % phenoxy dextran (DexP) in water, incubation with 0.1% Tween20 to block any naked/bare sites on SWNTs to prevent any non-specific adsorption and finally with 14 µM ConA solution prepared in 10 mM phosphate buffer supplemented with 0.5 mM CaCl2 and 0.1 mM MnCl2 (PB) for 2 h at room temperature. ConA being a metaloprotein requires transition metal ions, manganese and calcium, for its binding [65]. Because dextran cannot bind to the SWNTs by itself, hydrophobic dextran derivative, phenoxy dextran (DexP), was synthesized to noncovalently modify the SWNTs [23]. The fabrication and sensing processes were monitored by recording the current-voltage (I-V) characteristics between +1V to -1V of the device after each step using a semiconductor parameter analyzer. As shown in Figure 3.2, the current at the same corresponding voltage of the SWNT device decreased upon incubation with both dextran and ConA. The first decrease is a consequence of the modification of SWNTs with the DexP molecules by means of pi-pi stacking interactions between SWNTs and phenoxy groups and the latter is attributed to accumulation of the positive charge on the ConA molecules and/or a scattering potential effect resulting from its binding to dextran [66–68].

To examine the displacement principle of detection and functionality of the biosensor for glucose, the biosensor was incubated with 1 nM glucose in PB for 1 min, washed three times with PB followed by once with deionized water and the I-V was recorded. As shown in Figure 3.2, the conductance of the device reverted to the original value of dextran-modified SWNTs, confirming the displacement sensing modality for the weakly charged and small size glucose. Specificity of the biosensor was also evaluated by measuring the response of DexP and Tween20 blocked SWNTs without conjugated ConA for glucose, Mg2+, and Ca2+. As shown in Figure 3.3 the sensors conductance remained unaffected when incubated with 1 nM of glucose, 0.1 mM MnCl2 and 0.5 mM CaCl2 in 10 mM phosphate buffer, confirming the sensor response a result of highly specific competition between dextran and glucose for ConA binding sites. Figure 3.4 A shows normalized response [(R – R0)/R0, where R is the resistance after exposure to glucose and R0 is resistance after exposure to buffer determined from the inverse of the slope of the I-V curve from +0.1 V to -0.1 V] of the biosensor as a function of analyte concentration in buffer. The response was linear in the range of 1 pM to 1 nM and 0.039 per pM glucose (slope of the calibration plot) sensitivity. This lower detection limit is superior than the 50 nM and 3.7 mM reported for ConA-cyclodextrin/dextran solution based assays using fluorescence resonance energy transfer between CdTe quantum dot and gold nanoparticle [69] and infrared absorbance of carbon nanotubes deaggregation [23], respectively, and is attributed to the high sensitivity of chemiresistive/FET mode of transduction.

The biosensor selectivity was evaluated against sugars, sucrose and galactose. As illustrated in Figure 3.5, a two-fold higher concentration (2 nM) of sucrose, a disaccharide of glucose and fructose, was required to return the device resistance to the original value. On the other hand, there was no decrease in the device resistance when incubated with 1 nM monosaccharide galactose. However, when the same sensor was treated with 1 nM glucose, ConA was completely displaced from the sensor surface, confirming the sensor functionality. These selectivity results are in agreement with the literature [61] that ConA has lower affinity to sucrose in comparison with glucose and no affinity for galactose. Mechanism of operation of sensor although well proven, these sugar specificity tests further augment this fact. Furthermore, a nearly identical sensitivity when analyzing glucose spiked in human plasma (Figure 3.4B) demonstrated no interference from plasma components, i.e. no matrix effect, and potential application of the sensor for blood glucose measurement.

To conclude, we have built a SWNTs-based sensor displaying novelty in two aspects: first, the adaptation of the displacement mode of biosensing with chemiresistive sensor for detection of small molecules which otherwise are difficult to detect by chemiresistive/FET transduction principle and second, an enzyme-free chemiresistive glucose sensor with sensitivity in the picomolar range and exquisite selectivity. The ability to detect such low glucose concentration the reported sensor would find potential applications in monitoring glucose in unconventional body fluids such as interstitial fluid extracted by iontophoresis, tears, saliva and urine and intracellular

concentration at single cell level in metabolomic studies [10], [11], [70–73] While the displacement detection principle was demonstrated for glucose, it can also be applied to large weakly or uncharged molecules. Furthermore, the biosensor sensitivity can be amplified by augmenting the charge of the displacing moiety.

Legends to Figures

Figure 3. 1. Schematic of displacement-based chemiresistive biosensor.

Figure 3. 2. I-V characteristics of the biosensor at various stages of fabrication and upon addition of glucose.

Figure 3. 3. Response of SWNTs modified with DexP and Tween20 minus the ConA to 1 nM glucose, 0.1 mM MnCl2 and 0.5 mM CaCl2 prepared in 10 mM phosphate buffer.

Figure 3. 4. Biosensor calibration for glucose in 10mM phosphate buffer (A) and in human plasma (B). Data points are average of four independent sensors (for each investigation) prepared at different times and error bars represent ±1 standard deviation. Regression coefficient for the buffer sample is 0.97 and for spiked plasma sample is 0.98.

Figure 3. 5. Biosensor selectivity for various sugars (1 nM in 10mM phosphate buffer). Data points are average of 3 independent sensors prepared at different times and error bars represent ±1 standard deviation.

Figure 3. 1

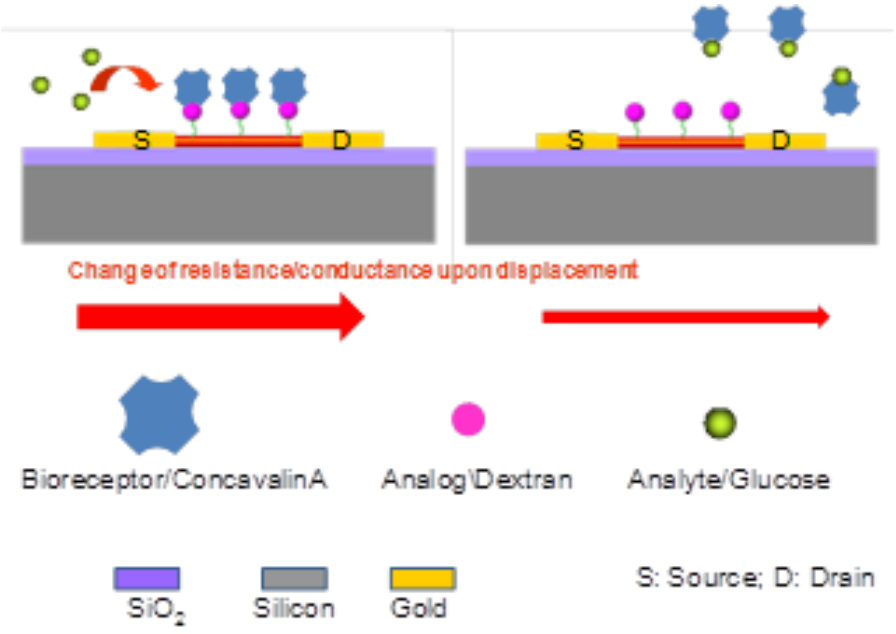
S
D
S
D
Change of resistance/conductance upon displacement
Bioreceptor/ConcavalinA
Analog\Dextran
Analyte/Glucose
SiO_2
Silicon
Gold
S: Source; D: Drain

Figure 3. 2

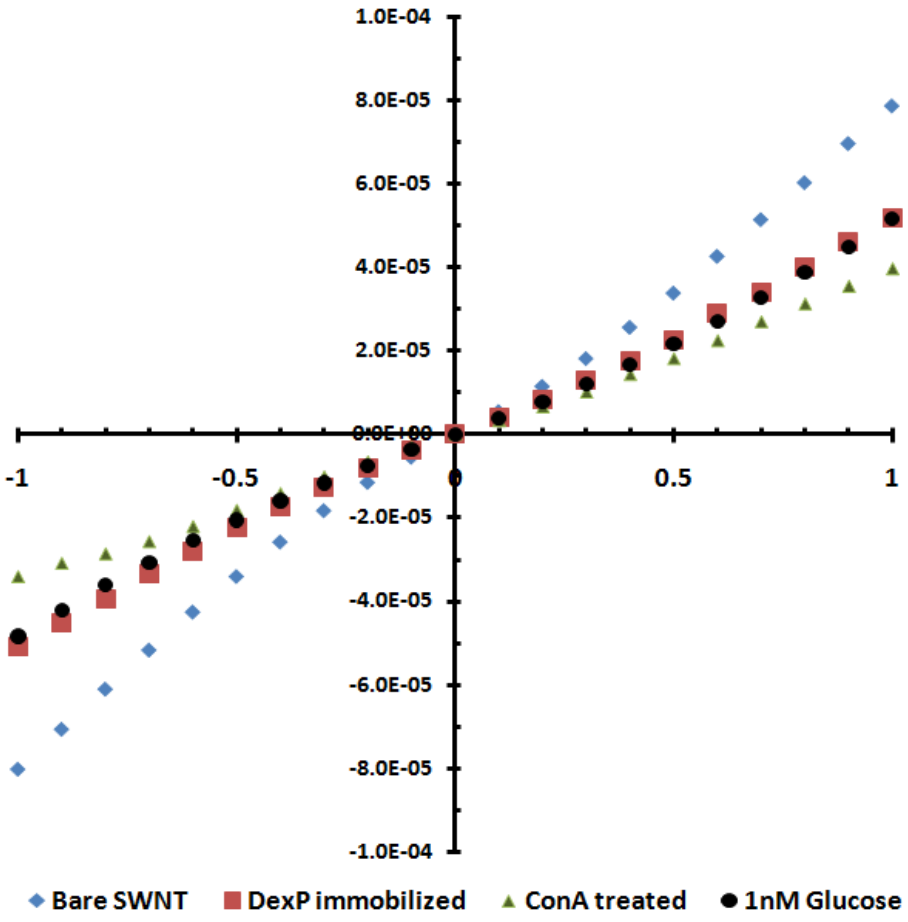
1.0E-04
8.0E-05
6.0E-05
4.0E-05
2.0E-05
0.0E+00
-2.0E-05
-4.0E-05
-6.0E-05
-8.0E-05
-1.0E-04
-1
-0.5
0
0.5
1
Bare SWNT
DexP immobilized
ConA treated
1nM Glucose

Figure 3. 3

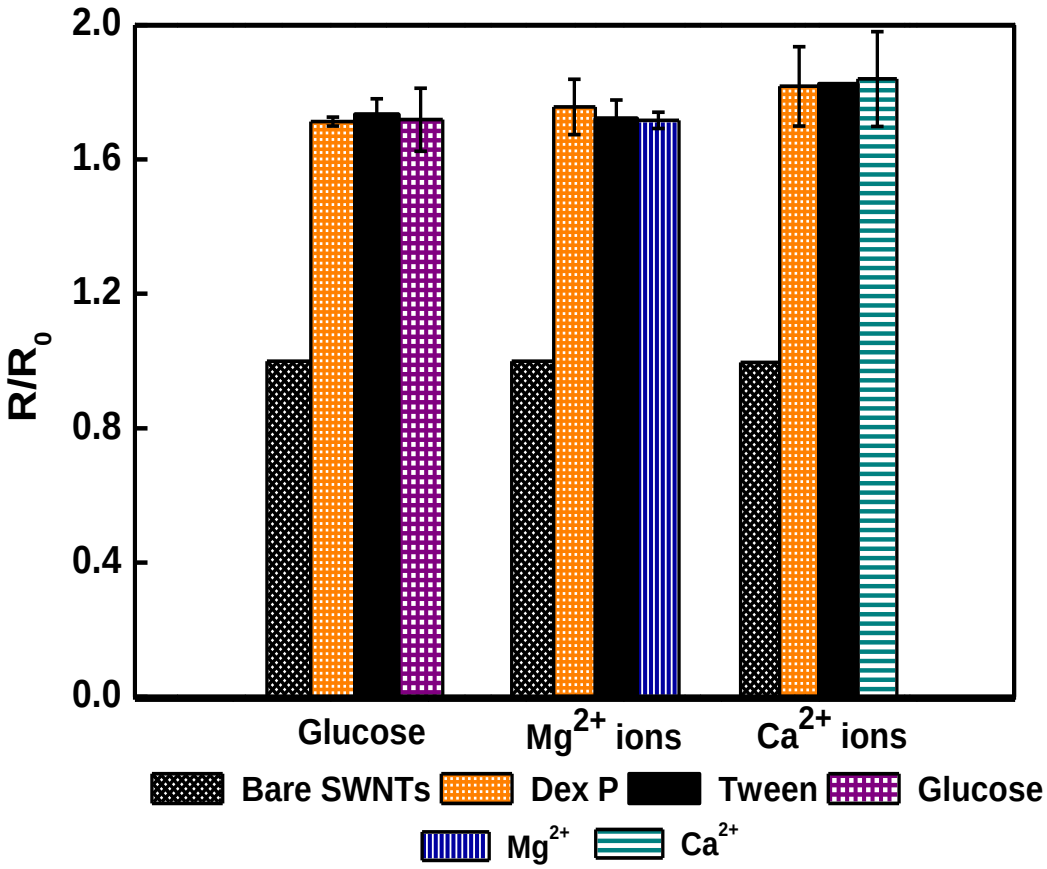
2.0
1.6
1.2
0.8
0.4
0.0
R/R0
Glucose
Mg2+ ions
Ca2+ ions
Bare SWNTs
Dex P
Tween
Glucose
Mg2+
Ca2+

Figure 3. 4

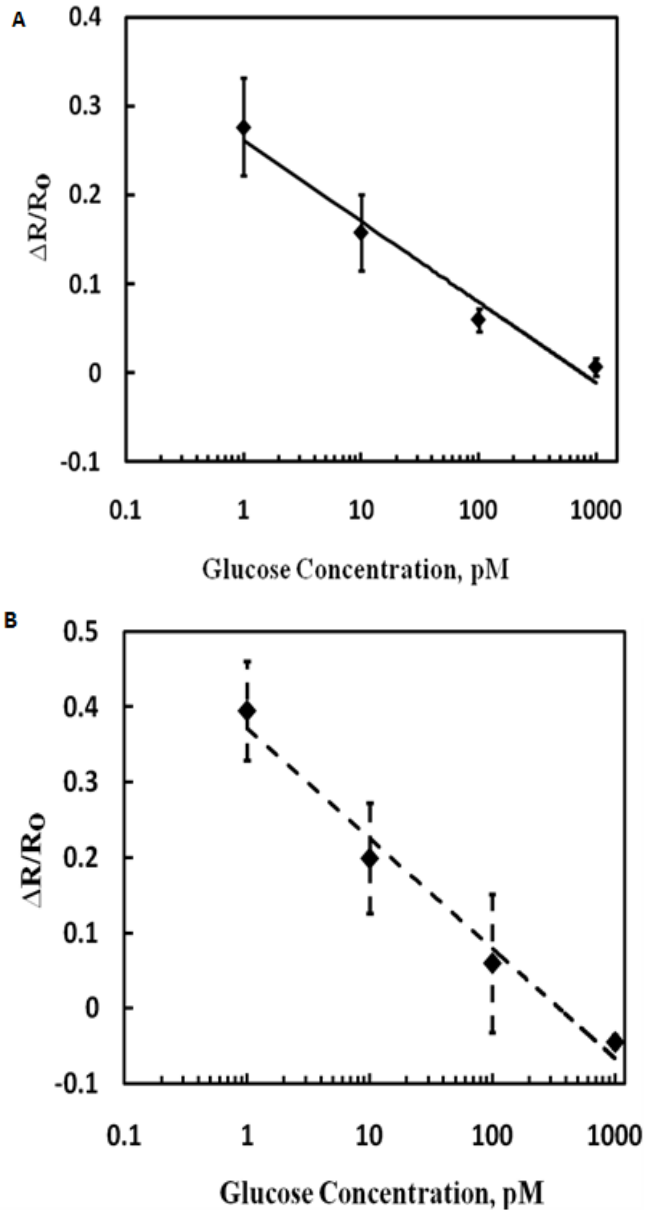
A
0.4
0.3
0.2
0.1
0
-0.1
ΔR/Ro
0.1
1
10
100
1000
Glucose Concentration, pM
B
0.5
0.4
0.3
0.2
0.1
0
-0.1
ΔR/Ro
0.1
1
10
100
1000
Glucose Concentration, pM

Figure 3. 5

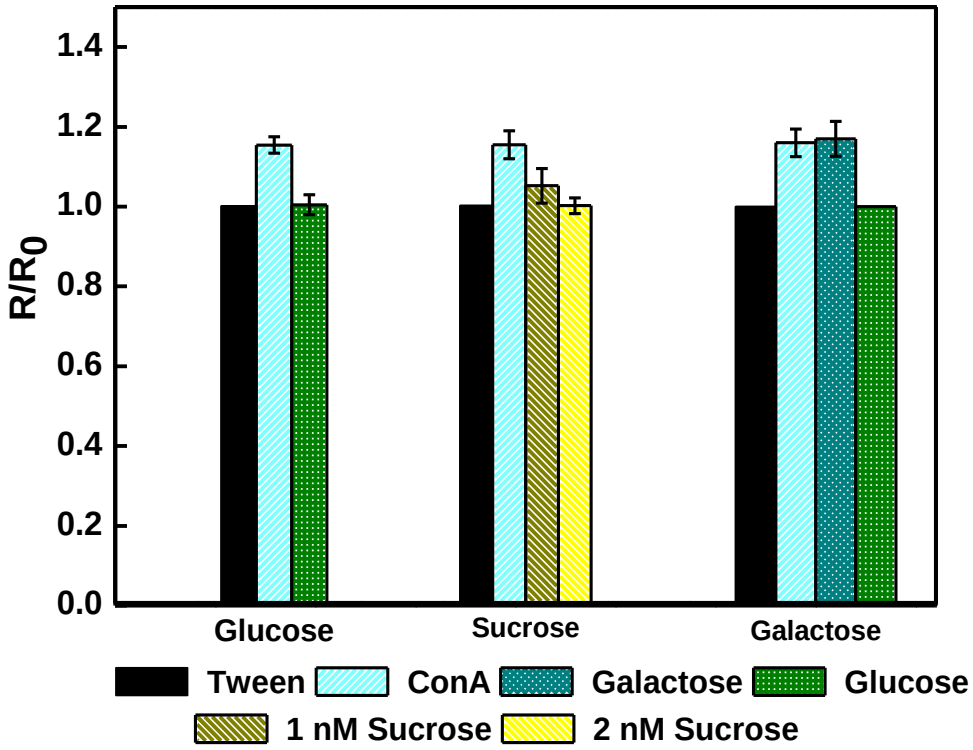
1.4
1.2
1.0
0.8
0.6
0.4
0.2
0.0
R/R0
Glucose
Sucrose
Galactose
Tween
ConA
Galactose
Glucose
1 nM Sucrose
2 nM Sucrose

Chapter 4:

Quantitative Assessment of in Vivo HIV Protease Activity Using Genetically Engineered QD-Based FRET Probes

Abstract

HIV protease plays a central role in its life cycle leading to release of functional viral particles. It has been successfully used as a therapeutic target to block HIV infection. Several protease inhibitors (PIs) are currently being employed as a part of anti-HIV therapy. However genetic drift in the virus due to constantly accumulating mutations including the protease leads to resistance and failure of therapy. We have developed quantum dot (Qdot)-based fluorescence resonance energy transfer (FRET) probes sensitive to HIV protease. These FRET probes consist of known HIV protease cleavage site sequences, Qdot as the fluorescence donor and alexa as the acceptor moiety. We have built *in vivo* assays by delivering this probe inside the cells for detecting HIV protease activity. Quantitative assessment of the HIV protease activity toward different cleavage sites *in vivo* has been recorded and can be used to gain insight into the protease, substrate and inhibitor interactions. Apart from assessing the wild type HIV protease activity against the wild type cleavage sites, we have been able to mimic the drug resistance causing mutations in protease as well as the cleavage sites. The changed IC50 values for the PIs recorded from this assay are similar to that observed in patients, validating our assay to be a better system for PI screening in future than the *in vitro* assays.

Introduction

Human Immunodeficiency Virus (HIV) is the causative agent of acquired immuno deficiency syndrome (AIDS). It belongs to the *retroviridae* family containing two identical copies of positive sense RNA genome enclosed in a protein cage. The HIV virology has been a topic of great interest for a long time and significant information regarding the various aspects of its life cycle through host cells has been acquired. This crucial information helps in developing targeted therapies to block the infection and also in development of sensitive and reliable diagnostic tools.

HIV life cycle is illustrated in figure 4.1. It starts with binding of the virus protein (gp120 and gp41 complex) to the CD4 receptor found on host T-cells, responsible for immune response in the body. Upon binding and interaction with specific co-receptor, the viral membrane and the host cell membrane fuse, releasing the capsid into the host cytoplasm (A). The viral capsid uncoats releasing the RNA (B). A double stranded DNA copy of the viral RNA(proviral DNA) is made with the help of viral reverse transcriptase and is transported into the nucleus to be integrated into the host genome by viral integrase enzyme (C and D). Upon cell activation messenger RNA (mRNA) of the proviral DNA occurs and is transported out into the cytoplasm for translation (E). The mRNA is translated into two long polyprotein fragments called the gag and gag-pol polyproteins (F). A protease enzyme, part of the gag-pol polyprotein auto-catalytically releases itself

and further processes the rest of the polyprotein in an ordered fashion releasing all the individual viral proteins (G). These proteins assemble along with the two copies of RNA into a mature HIV virion and released out of the cells (H) through budding. The HIV life cycle provides it with a significant advantage for survival at several stages: Firstly it attacks the T-cells central to the host immune response[74], secondly the HIV reverse transcriptase enzyme lacks proof reading activity and incorporates several mutations leading to development of resistance in the virus against the current drug therapy[75][76] and lastly by integrating the proviral DNA into host they become a part of host and can remain latent for several years before being activated by yet to be determined stimulus[77].

HIV protease plays a central role in formation infectious viral particles. It belongs to the family of aspartic proteases and is a homodimer of subunit made of 99 amino acids[78]. Due to the important role of HIV protease in its life cycle and its structural understanding has made it a great target for anti-HIV therapy. Currently there are nine different protease inhibitors(PIs) currently approved for patient treatment: saquinavir (SQV), ritonavir (RTV), indinavir (IDV), nelfinavir (NFV), amprenavir (APV), lopinavir (LPV), atazanavir (ATV), tripranavir (TPV) and darunavir (DRV). These inhibitors mimic the natural substrate for the HIV protease and have shown to be very effective in blocking its function mostly by binding to the active site [79-85] and in certain cases preventing the dimerization[80].

However owing the PI pressure, drug resistance HIV variants emerge due to the multiple mutations in the protease, leading to treatment failure. These mutations also cause severe cross resistance to other PIs which may not be a part of the anti-HIV therapy of a patient. Development of PI resistance starts with specific mutations at residues involved in inhibitor binding, called the primary mutations[81]. These mutations affect the HIV replication ability as well due to change in the substrate binding environment. In order to compensate for the reduced viral fitness secondary mutations develop both in the protease as well as protease substrate sequences of gag and gag-pol polyproteins[82][83]. There have been reports claiming certain mutations in gag polyprotein at the site NC-p1 can lead to resistance even in absence of corresponding protease mutations. NC-p1 is a gag cleavage site, hydrolyzed the slowest by HIV protease making it a rate limiting step and making it an attractive target for accumulations of mutations to compensate for loss in viral fitness[84].

Several assays have been developed for identification of new inhibitors against HIV protease and majority of these are *in vitro* assays based on purified enzyme and generalized peptidic substrates. Cell based assays or *in vivo* assays are an alternative to *in vitro* assays and confer several advantages. They utilize cell based environment with enzyme in natural confirmation and also the substrate mimicking specifically the natural cleavage sites for the protease. These PI screening assays apart can be very well applied for diagnostic applications. They also will provide preliminary information with regard to toxicity of the compounds identified [85].

Our lab has constructed a protein module for in vivo monitoring of HIV protease activity based on fluorescence resonance energy transfer (FRET)[86]. The probe design is illustrated in Figure 4.2. The N terminus contains a HIS-tag that can be used to conjugate to a quantum dot (Qdot) surface through metal affinity interactions. Qdots are luminescent and act as a FRET donor. The HIV protease substrate sequence is derived from the original cleavage site sequence of gag and gag-pol polyproteins. Elastin like polypeptide (ELP) module helps in temperature based purification of the probe. ELP displays temperature phase transition properties. It is completely soluble at a temperature lower than the transition temperature and aggregated at the temperature above it. The transition temperature of ELP can be modulated by addition of salt into the ELP solution. It has also been shown that the higher ELP concentration leads to better purification. By fusing the protein of our interest to the ELP, temperature can be altered to above the transition temperature [87]. This leads to aggregation and falling out of ELP fusion protein alone and can be collected by centrifugation. The tat module helps in delivering the probe *in vivo* [88][89]. A unique cysteine residue is incorporated between the cleavage sequence and the ELP domain for unique conjugation of alexa fluorescent dye through thiol malemide reaction. This alexa dye acts as fluorescence acceptor. Upon excitation of Qdot, due to the spectral overlap and close proximity to alexa dye, energy is transferred and alexa dye is excited. The fluorescence emission collected would be from Alexa rather than Qdot. In the presence of protease the probe is cleaved and the Qdot and Alexa are separated to distance wherein energy transfer

cannot happen and thus the emission collected would be from Qdot. Successful detection of HIV protease activity *in vivo* has been demonstrated and quantitative assessment of inhibitor activity has been shown.

Numerous studies report the kinetic parameters for HIV protease *in vitro* using a random hydrolysable substrate [90] or MACA substrate sequence. These kinetic parameters along with the structural information have led to a better understanding of substrate hydrolysis and PI mode of action. A number of these *in vitro* assays have been utilized for screening of new inhibitors, however most of the candidate molecules failed in early clinical trials indicating the lack of discretion in these assays. Thus *in vivo*/cell based assays which are a closer mimic of the natural environment encountered by HIV protease make a better system for identifying new PIs. These assays can provide preliminary information regarding permeability and toxicity of the PI candidates. A number of cell based assay systems are reported but our assay system with the FRET probe provides a number of advantages over them [91–94]. Our assay does not require any transgenic lines expressing reporter protein sensitive to HIV protease, HIV substrate sequence employed in our probe mimics the natural polyprotein cleavage sequence and can be easily replaced with a new cleavage site. Our assay can provide assessment of HIV protease activity in vivo for multiple substrates including mutant cleavage sites, information regarding which is lacking. We can further introduce drug resistance mutations identified in patients into the protease and gain a better understanding of the PI therapy failure and cross resistance pattern. The flexibility of our assay can be utilized

to establish a high throughput screen (HTS) for identifying newer PIs for the wild type as well as mutated forms of the virus.

Materials and Methods

Materials:

TOPO capped Qdot® 545 ITK™ Organic Quantum Dots (Qdot 545), Alexa Fluor® 568 C5 maleimide (Alexa 568) and Tris-(2-carboxyethyl) phosphine (TCEP) were purchased from Life technologies. Di hydro Lipoic acid (DHLA) was purchased from Sigma Aldrich. HeLa cells were obtained from American Type Culture Collection. Autoclavable minimum essential medium was from Irvine Scientific. Cell culture grade NaHCO3, Hepes, nonessential amino acids, penicillin and streptomycin L-glutamine was purchased from HyClone, Thermo Scientific. Fetal Bovine serum (FBS) was purchased from Sigma Aldrich. Restriction enzyme, Ligase and Polymerase enzymes were obtained from New England Biolabs (NEB).

Design of Constructs:

The pET14b expression vector for His6-MA/CA-Cys-ELP105K-TAT (H-MA/CA- ET) was obtained from Payal Biswas et.al., [86]. To make the other cleavage site variants an artificial gene carrying hexa-histidines and the NC-p1 wild type peptide with cysteine was ordered from Integrated DNA Technologies (IDT) with sequences CAT GGG CCA TCA CCA TCA CCA TCA CAC CGA ACG CCA GGC GAA CTT TCT GGG CAA AAT TTG GCC GTG CCA and TAT GGC ACG GCC AAA TTT TGC CCA GAA AGT TCG CCT GGC GTT CGG TGT GAT GGT GAT GGT GAT GGC C . The two oligos are mixed at equimolar concentrations and

annealed together by heating to 95^0 C for 5 min and cooling gradually. The MA-CA fragment is removed by digesting pET-H-MA/CA-ET with Nde1 and Nco1 and the new oligo also digested by Nde1 and Nco1 is ligated overnight to get pET-H-NC/p1 WT-ET. Similar procedure was followed to obtain the mutant cleavage site variant using oligos CAT GGG CCA TCA CCA TCA CCA TCA CAC CGA ACG CCA GGT GAA CTT TCT GGG CAA AAT TTG GCC GTG CCA and TAT GGC ACG GCC AAA TTT TGC CCA GAA AGT TCA CCT GGC GTT CGG TGT GAT GGT GAT GGT GAT GGC C. The plasmid is called pET-H-NC/p1 M2-ET.

Expression and purification of peptides

The expression cell line, *E.coli* BL-21(DE3) (Novagen, Madison, WI) were transformed with plasmids pET-H-MA/CA-ET, pET-H-NC/p1 WT-ET and pET-H-NC/p1 M2-ET. All the three cell lines were grown in terrific broth media containing 100 μg/ml ampicillin at 37^oC until an optical density (O.D) of 0.5 was reached and then they were transferred to 30^0 C shaker incubator at 280 RPM. The cells were harvested at the end of 12 hrs by centrifugation and the pellet resuspended in 50mM Tris/HCl (pH 8.0) with 0.1M NaCl and 1 mg/ml of lysozyme. The cells were lysed by sonication (Thermo scientific) and the cell debris was removed by centrifugation at 16,000 g for 30 min. The purification of proteins from the clarified supernatant involves addition of NaCl to a final concentration of 2N and warming up the solution in 37^0 C water bath. The solution becomes cloudy due to ELP aggregation and was collected by centrifugation at 30^0 C and 16000 g. The ELP protein containing pellet was resolubilized in the sonication buffer and centrifuged

at 4^0 C for 30 min at 16000g to remove any contaminating proteins. The peptides in the supernatant are again precipitated by adding NaCl to a final concentration of 2N and centrifugation. The peptide pellets were stored at -20^0 C and resuspended in 50mM Tris/HCl (pH 8.0) with 0.1M NaCl [95]. The purity of the protein was confirmed through SDS-PAGE gel electrophoresis and concentration determined through absorption at 215 nm (Inverse extinction coefficient 280).

Fluorescent dye conjugation:

The labeling of the proteins was carried out as per the vendor instructions. Purified proteins were resuspended in 50mM potassium phosphate buffer (pH 7) at a final concentration of 200 µM along with 10-fold excess TCEP in a final volume of 1000 ul. The solution was incubated at room temperature on a rotator for 6 h and 10- fold excess Alexa 568 maleimide was added followed by incubation at room temperature for two hours on a rotator. The solution was then transferred to a 4^0 C refrigerated rotator and incubated for 16 h. At the end of incubation period the unreacted dyes were removed by two or three thermal precipitation cycles similar as described above. The degree of labeling was estimated by

$$\frac{A_x}{E} \times \frac{Mol\ Wt\ of\ the\ protein}{mg\ protein/mL} = \frac{Moles\ of\ dye}{Moles\ of\ protein}$$

Where A_x is the absorbance value of the dye at 568 nm and E is the molar extinction coefficient of 92000 cm^{-1} M^{-1}.

Qdot conjugation of Alexa labeled peptide:

The conjugation of QDs to fluorophore-labeled protein module to complete the FRET pair was adapted from Clapp et al., 2006 [96]. The TOPO-capped CdSe/ZnS QD 545 obtained in decane are initially flocculated and resuspended in toluene as per manufacturer's instructions followed by water solubilization by exchanging the TOPO cap with DHLA. 300 nM of DHLA-capped QDs were mixed with required molar ration of Alexa labeled proteins, resuspended in 10mM HEPES buffer (pH 8.2) and incubated at room temperature on a rotator for 12 h. The conjugation confirmation is obtained by measuring the FRET efficiency using a fluorometer by exciting at 430 nm and recording the spectrum from 500 nm to 700 nm.

Cell culture:

HeLa cells were cultured in T-50 flasks. 1X minimum essential medium containing 1% of 7.5% $NaHCO_3$, 2% of 1 M Hepes, 1% of nonessential amino acids, 100 µg/mL of penicillin and 100 U/mL of streptomycin, 1% of 200 mM L-glutamine in 0.85% NaCl, and 10% of FBS was used as the growth medium and cells were cultured at 37°C and 5% CO_2.

Intracellular probe delivery, transfection and PI application

HIV infection and production of the HIV protease is achieved through a plasmid system (pNL4-3.HSA.R-E-) with sequence of wild type HIV-1 strain (HXB2). Upon transfection of mammalian cells with this plasmid all functional components of the virus are expressed.

However due to two mutations in the env and vpr gene, they do assemble to complete viral particles and are not released into the medium [97][98]. HeLa cells were seeded into 96 well clear bottom black wall side plates and grown to 80 % confluency at 37°C and 5% CO2. The spent media was aspirated and Qdot conjugated protein diluted to 150 nM Qdot concentration in 1× Leibovitz L-15 medium was added to the wells. The plate was incubated for 2 hr at 37^0 C in dark. The probe solution was aspirated and cells were washed twice with PBS. At the same time the proviral plasmid pNL4-3.HSA.R-E- was diluted to opti-MEM media. Similarly Lipofectmine™ 2000 was diluted in opti-MEM to concentrations reported by the manufacturer. The lipofectamine and plasmid were mixed together and added to each well to a final concentration of 100 ng plasmid. The cells were incubated at 37^0 C for 6 h following which the transfection media was replaced by growth media. In case of inhibitor experiments, the cells after Qdot conjugated probe delivery were incubated with growth media containing respective concentrations of PIs for four hours following which transfection was carried out. After transfection the replaced growth media also contained PIs are required concentration. The percentage inhibition efficiency was calculated from the quantified FRET/Qdot values for three random regions according to the formula

$$\%\, Inhibition\ efficiency = \frac{(FRET|Qdot)_{inhibitor} - (FRET|Qdot)_{No\ inhibitor}}{(FRET|Qdot)_{control} - (FRET|Qdot)_{No\ inhibitor}}$$

Site directed mutagenesis

The protease region (PR) of the pNL4-3.HSA.R-E- was amplified by using primers: PR-***EcoRI***/Sph1 Forward: 5' AGT***GAATTC***GCATGCAGGGCCTATTGCACC 3' and PR-***Xba1***/Age1 Reverse:

5' ***TCTAGA***CCGGTTCTTTTAGAATCTCCC 3'. The amplified product was digested with EcoR1 and Xba1 and cloned into corresponding restriction sites of pBlueScript –SK+ (Stratagene, La Jolla, CA) and the plasmid called pBSk-PR. The protease mutations identified were introduced into pBSK-PR using the Quickchange Site-Directed Mutagenesis Kit (Stratagene) using the manufacturer's instructions. Primers for mutagenesis were ordered from Integrated DNA Technologies (IDT). The primers for introducing mutation at 82nd location of the PR (V82A) are: V82A Forward: 5'-tattagtaggacctacacctgccaacataattggaagaaatctg-3' and V82A Reverse 5'-cagtattagtaggacctacacctgtcaacataattggaagaaatctgttg -3'. The primers for introducing mutation at the 90th location of PR (L90M) are: L90M Forward 5'-cataattggaagaaatctgatgactcagattggctgcac-3' and L90M Reverse 5'-caacataattggaagaaatctgttgactcagattggctgcacttt-3'. After the PCR based mutation introduction and cloning the palsmids containing mutated protease – pBSK-PR-V82A and pBSK-PR-L90M are isolated and digested with Sph 1 and Age 1 and ligated back into the pNL4-3.HSA.R-E- digested with the same enzymes. The mutations were confirmed by

sequencing and large scale DNA preparation of the mutants: pNL4-3 –V82A and pNL4-3 –L90M was performed using Qiagen maxi prep kit.

Fluorescence Microscopy and image processing

Cell imaging was performed on a Axio observer z1 motorized inverted research microscope. The objective used was LD Plan-Neofluar 20x/0.4Ph2CorrWD=8.4M27 from Ziess. Fluorescent probes were detected by using two different filter sets; QD filter consisting of a D436-nm exciter, a D535/50-nm emitter, and a 475 nm-dichroic long pass beam splitter (Chroma Technology) and FRET filter consisting of ET450/50x, ET595/40m and T495LPXR, 25mm diameter excitation and emission filters, 25.5x36mm dichroic. Images were acquired by using Axio –vision software from Ziess and fluorescence images were analyzed by using Image-Pro PLUS analysis software (Media Cybernetics). Quantification was done by estimating the mean intensity of Qdot image and FRET image, for three random fields in each well using Image-Pro PLUS analysis software.

In vivo probe concentration estimation

The HeLa cells were delivered with Qdot conjugated probes at varying peptide to Qdot ratios and the quantification of the images performed as described above. Based on the amount of protein delivered in the form of conjugate per well, the approximate number of cells per well and the average volume of HeLa cells at their confluency stage, the *in vivo* probe concentration was calculated and correlated to the quantified FRET image intensity to Qdot image intensity(FRET/Qdot). Thus obtained calibration was used for

further experiments to calculate the *in vivo* concentration of intact probe from the FRET/Qdot numbers. The exposure time for the fluorescence images was maintained constant for a particular probe and between calibration and actual experiments.

Results and Discussion

FRET characterization

The MACA-Alexa labeled protein was incubated at different molar concentrations was conjugated with fixed concentration of Qdot 545. The ratio of MACA-Alexa to Qdot is represented by n. Figure 4.3. shows the fluorescent spectra at different values of n and clearly demonstrates the FRET occurrence with increasing n. The saturation of the Qdot surface was confirmed by running the conjugate samples on a SDS-PAGE and the saturation ratio was determined to be 40.

Fluorescence resonance energy transfer is a result of nonradioactive energy transfer between the donor and acceptor in close proximity. The efficiency of the energy transfer(E) is dependent on the center to center distance between the donor and the acceptor (r)and requires a nonzero integral value(I) for donor emission and acceptor absorption spectral overlap [99]. The Forster distance, which is the center to center distance where in the energy transfer efficiency is 50%, was calculated based on previously published theory according to equation 1 [100].

$$R_0 = \frac{9000(\ln(10)k_p Q_D}{N_A 128\,\pi^4 n^4} \ldots\ldots\ldots\ldots\ldots\ldots\ldots\ldots\ldots\ldots\ldots\ldots 1$$

Where k_p depends on orientation of donor and acceptor dipoles and k_p^2 is 2/3 for randomly oriented dipoles, N_A is the Avogadro's number, n_D is the refractive index of the medium and Q_D stands for quantum yield. The overlap integral, I depends on the

normalized donor emission spectra (PL_D) over wavelength λ and acceptor absorption spectrum (E_A) (Equation 2)

$$I = \int_0^\infty PL_D(\lambda) \times \lambda^4 \times \in_A (\lambda) \quad \text{.....2}$$

The FRET efficiency E, is determined based on equation 3 from experimental data

$$E = 1 - \frac{F_{DA}}{F_D} \quad \text{.....3}$$

Where F_{DA} is the integrated fluorescence intensity of the donor in presence of acceptors and F_D is of the donor alone. The actual separation distance, r between Qdot 545 and Alexa 568 was calculated according to equation 4,

$$r_n = R_0 \left(\frac{n(1-E)}{E}\right)^{1/6} \quad \text{.....4}$$

The calculated Forster distance for our system is 52.4 Å and the separation distance is 57.9±8.7 Å (Figure 4.4).

In vivo probing of HIV protease activity

The Qdot-MACA Alexa conjugate at Alexa to Qdot ratio of 40 was delivered into the cells by incubating for 2h. The cells were then washed and transfected with the HIV proviral plasmid pNL4-3.HSA.R-E- for 6h. The fluorescence changes in the control wells (no transfection) and the transfected wells were captured temporally under the microscope (Figure 4.5). The fluorescence captured from control wells was at the alexa emission (red) and indicated the integrity of the probe delivered. However the fluorescence in the

transfected wells gradually shifts from the Alexa emission (red) to Qdot emission (green) indicating the probe hydrolysis by HIV protease. The fluorescence images were merged with bright filed images and the site of probe hydrolysis was confirmed to be inside the cells. In order to verify the specificity of this system, a nonspecific probe (West Nile Virus protease cleavage substrate – Qdot-WNV-Alexa) synthesized, labeled and conjugated in the similar fashion of MACA probe, was delivered and the fluorescence changes monitored. As shown in figure 4.6, the Qdot-WNV-Alexa control and transfected wells did not show any fluorescent changes even at 18h post transfection as opposed to Qdot-MACA-Alexa delivered wells.

Since the fluorescence (FRET/Qdot) changes over time indicate HIV protease activity, by expressing the FRET/Qdot changes in terms of intact probe concentration inside the cells, probe hydrolysis rate can be estimated. In order to do so we delivered conjugates with varying number of MACA-Alexa per Qdot (n) and quantified FRET/Qdot for each n (Figure 4.7 A). Using the probe concentration delivered, the number of cells per well and the average volume of HeLa cell at confluency, we converted the FRET/Qdot ratios to intact probe concentration in vivo (Figure 4.7 B). Figure 4.8 A is the quantified FRET/Qdot changes over time for MACA probe and figure 4.8 B is the intact MACA probe concentration at different time post transfection, the slope of which is the rate of MACA probe hydrolysis by HIV protease. The estimated initial probe concentration in vivo (38 mM) is in excess of reported affinity constant (K_m) for any of the natural substrates of

HIV protease [101][102][103]. Hence the rate we captured in our assay would be indicative of the maximum hydrolysis rate for MACA probe (V_{max} 284 nM s^{-1}) according to Michaels- Menten kinetics [104]. Also V_{max} is a product of total enzyme concentration (E_T) and turn over number (K_{cat}). In accordance to our theory of capturing V_{max} which is directly proportional to K_{cat}, our assay should be discriminatory of differences in K_{cat} values for different HIV protease substrate, if the assays performed under identical conditions (same E_T). We built a probe mimicking the NC-p1 cleavage site of the gag polyprotein as substrate sequence, labeled it with alexa and conjugated to Qdot (Qdot-NCp1-alexa). The NC-p1 substrate has a significantly lower K_{cat} compared to the MA-CA substrate [105][106]. A correlation plot of FRET/Qdot numbers with intact probe concentration for the new probe was estimated similar to the Qdot-MACA-Alexa probe. The Qdot-NCp1 –Alexa probe was delivered into HeLa cells and the fluorescence changes captured over time (Figure 4.9 A). The corresponding plot of changing intact probe concentration with time is shown in Figure 4.9 B. The slope, V_{max} for Qdot-NCp1 WT-Alexa hydrolysis as estimated from the curve was 22 nM s^{-1}, ≈13 fold lower than the Qdot-MACA-Alexa substrate. This difference estimated is comparable to the reported differences and the slightly faster processing of NCp1 substrate might be a result of our probe design and assay format.

The cleavage of NC-p1 site by the HIV protease has appeared to be rate limiting step [107] with the lowest specificity constants(K_{cat}/K_m) among all the cleavage sites [105].

This site has been identified in both in vivo and in vitro system to be one of the favored sites to mutate, along with protease mutations [108][39][40]. These mutations have been associated with PI resistance, alone and along with the protease mutations[84]. It's shown that the mutation at this site act as compensate for loss of viral fitness by increased catalytic efficiencies [105]. We identified a mutation in NC-p1 site (A431V) that resulted in K_{cat} values in comparison with the wild type site (figure 4.10 A). The probe Qdot-NCp1M2-Alexa was delivered into the HeLa cells in similar fashion to the wild type Qdot-NCp1-Alexa probe and fluorescence changes captured (figure 4.10 B). The quantified hydrolysis rate, V_{max} (22 nM s^{-1}) for this probe differed by 3.9 fold compared to the wild type (Figure 4.10 C).

To further prove the versatility of our system we incorporated point mutations into the protease region of the proviral vector, pNL4-3.HSA.R-E- with sequence of wild-type HIV-1 reference stain HXB2. These mutations are known to be associated with the NC-p1 cleavage site mutation as present in Qdot-NCp1M2-Alexa probe. Mutation V82A – replacement of Valine(V) at location 82 of the protease with Alanine(A), is known to be associated with the A431V cleavage site mutations [111]. Viruses with this combination of mutations are known to be resistant to PI indinavir with an average of 20 fold change in IC50 (concentration of the PI where virus in 50% of the population is inhibited) [112] . Mutation L90M - replacement of Leucine (L) at location 90 of the protease with Methionine (M), is another commonly found mutation in drug resistant viruses. This

mutation in combination with A431V results in increased resistance to all PIs, remarkably so with saquinavir (average IC50 change of about 10 fold)[112]. We introduced mutations V82A and L90M into the proviral protease region using site directed mutagenesis (figure 4.11 A). We ensured that the plasmid with mutations is still functional upon transfection using the Qdot-MACA-Alexa probe. The wild type (pNL4-3.HSA.R-E-/ HXB2) and mutants (V82A and L90M) hydrolyzed the MACA substrate with similar rates (figure 4.11 B) as this cleavage site is one of most efficiently processed cleavage sites [105]. Upon testing the wild type and mutant versions of the protease with the Qdot-NCp1M2 – Alexa probe, a marked difference in IC50 concentration of PI was identified (Figure 4.12 A and B). The IC50 values of inhibitors against the wild type and mutants we estimated are in accordance with the literature reports [112].

Conclusion

We have designed a modular FRET probe detecting HIV protease *in vivo* and demonstrated its flexibility as a cell based screen for identifying potential inhibitors. We have further extended this assay and report the ability to capture protease activity against different cleavage site in vivo, knowledge of which is very limiting. By working with combination of cleavage site mutation and corresponding protease mutation in our assay system we captured the increased resistance to PIs. The fold change in IC50 of the inhibitors is in accordance with the patient data. This validates the use of our assay for future screening of inhibitors and also for resistance testing purposes for newly infected patients. This assay can be used to isolate commonly found protease and cleavage site mutations and affirmatively confirm their contribution to the patient resistance pattern to a particular PI or a combination. Although we have shown single protease mutations and their effect, we can easily introduce multiple mutations and increase the scope of study.

Legends to Table

Table 4. 1: Tabulated values of reported and estimated IC50, for mentioned mutation and inhibitor combination.

Legends to Figures

Figure 4. 1. HIV life cycle. (A) Binding and entry, (B) uncoating, (C) Proviral DNA synthesis and transport into nucleus, (D) integration of the HIV proviral DNA into the host genome, (E) activation and synthesis of mRNA from proviral DNA and its transport into cytoplasm, (F) translation of the mRNA into gag and gag-pol polyproteins and release of protease from the gag polyprotein, (G) release of other viral proteins by action of the protease and their assembly into new virions and release (H).

Figure 4. 2. HIV protease sensitive protein FRET module.

Figure 4. 3. Fluorescence spectra obtained by conjugating varied protein (MACA-Alexa) molar concentrations with fixed Qdot concentration depicting the FRET.

Figure 4. 4. FRET characterization. E – FRET Efficiency, r – actual separation distance, R0 – Forster distance.

Figure 4. 5. Temporal capture of the Qdot-MACA-alexa protein probe in vivo

Figure 4. 6. Capture of fluorescent changes with Qdot-MACA-alexa probe and nonspecific Qdot-WNV-alexa protein in both control and transfected wells.

Figure 4. 7. A. The fluorescence images corresponding to the delivery of varying MACA-alexa protein to Qdot conjugated samples and B. the calibration plot correlating the fluorescence changes (FRET/Qdot) with in vivo probe concentration.

Figure 4. 8. A. Quantified fluorescence changes of Qdot-MACA-alexa probe processing over time, B. Corresponding plot of quantified changes in intact probe concentration vs time, the slope of which gives the Vmax

Figure 4. 9. A. Temporal capture of fluorescence changes of Qdot-NCp1 WT- alexa probe in control and transfected samples, B. Plot of quantified changes in intact probe concentration vs time, the slope of which gives the Vmax

Figure 4. 10. A. The sequence of the mutant NC-p1 site as opposed to the wild type, B. Temporal capture of the fluorescent changes of Qdot- NCP1 M2-alexa protein in control and transfected samples, C. Plot of quantified changes in intact probe concentration vs time, the slope of which gives the Vmax

Figure 4. 11. A. Amino acid residues of Wild type HIV-1 (HXB2) protease (above the bar) with their location (numbers within the bar) and the mutated residue (below the bar). The highlighted amino acid at where mutated by site-directed mutagenesis, B. The combined plot of changes in Qdot-MACA-alexa probe concentration in vivo with time in case of wild type protease (HXB2) and mutant HIV protease (V82A and L90M).

Figure 4. 12. A. Inhibition efficiency of indinavir in case of wild type (HXB2) protease and mutant (V82A) protease, B. Inhibition efficiency of saquinavir in case of wild type (HXB2) protease and mutant (L90M) protease, C. Tabulated values of reported and estimated IC50 values for mutation and inhibitor combinations.

Figure 4. 1

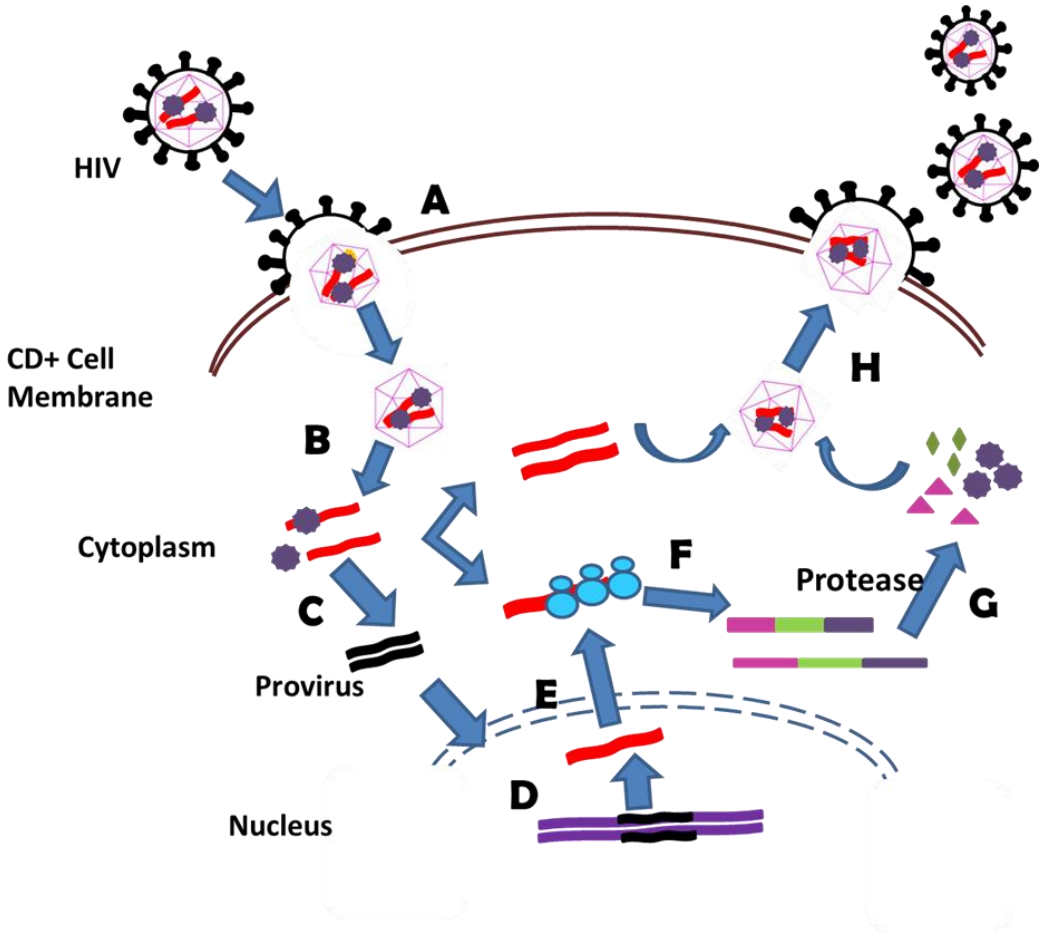
HIV
A
CD+ Cell
Membrane
B
Cytoplasm
C
Provirus
Nucleus
D
E
F
Protease
G
H

Figure 4. 2

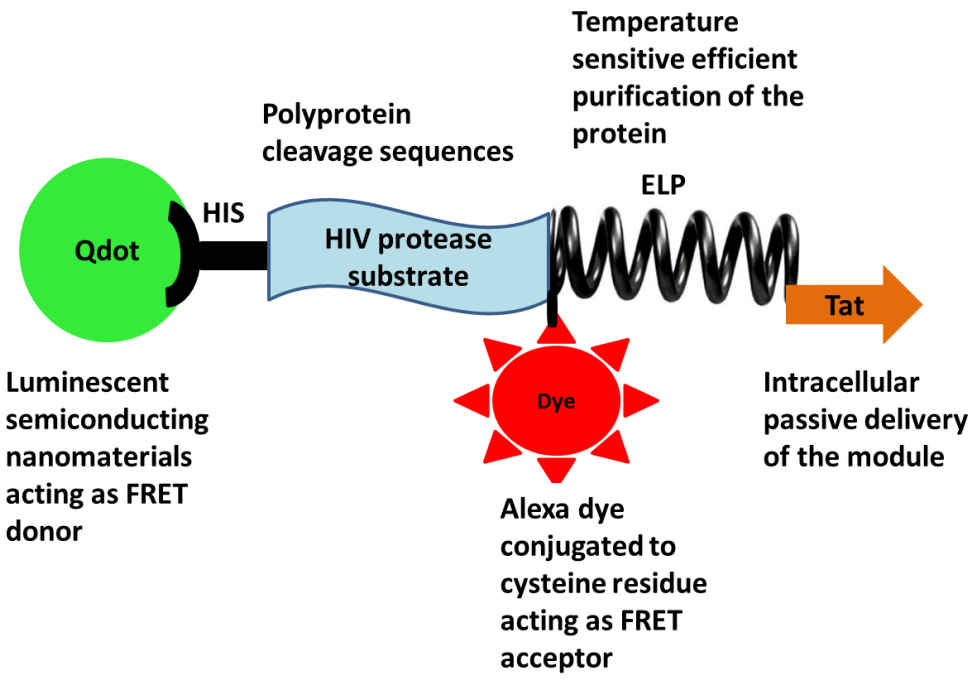
Temperature sensitive efficient purification of the protein
Polyprotein cleavage sequences
ELP
HIS
Qdot
HIV protease substrate
Tat
Dye
Luminescent semiconducting nanomaterials acting as FRET donor
Intracellular passive delivery of the module
Alexa dye conjugated to cysteine residue acting as FRET acceptor

Figure 4. 3

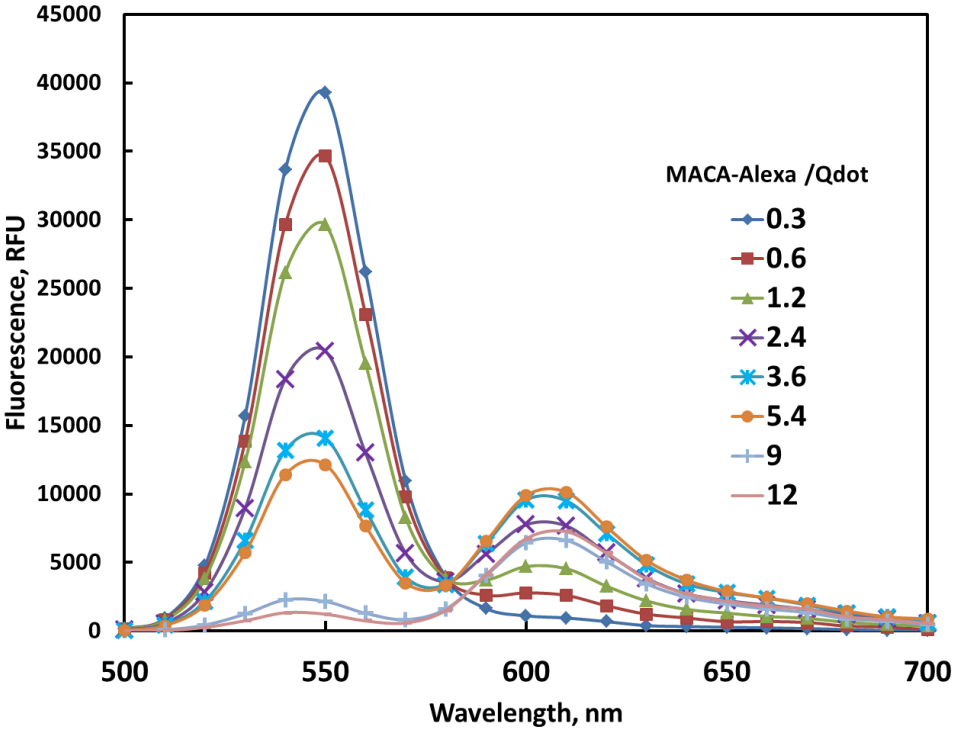
45000
40000
35000
30000
25000
20000
15000
10000
5000
0
Fluorescence, RFU
500
550
600
650
700
Wavelength, nm
MACA-Alexa /Qdot
0.3
0.6
1.2
2.4
3.6
5.4
9
12

Figure 4. 4

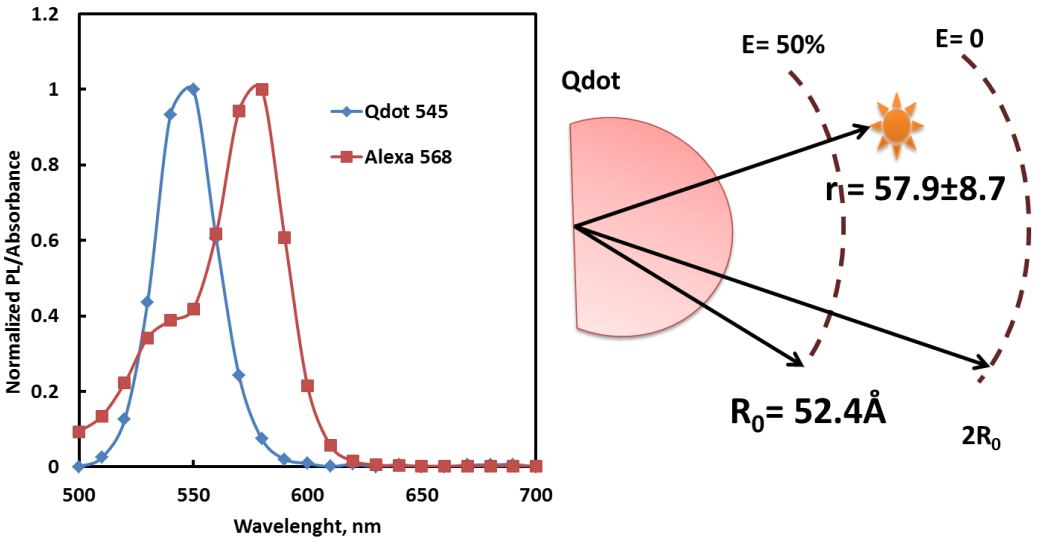
1.2
1
0.8
0.6
0.4
0.2
0
Normalized PL/Absorbance
500
550
600
650
700
Wavelenght, nm
Qdot 545
Alexa 568
Qdot
E= 50%
E= 0
r1= 57.9±8.7
R0= 52.4Å
2R0

Figure 4. 5

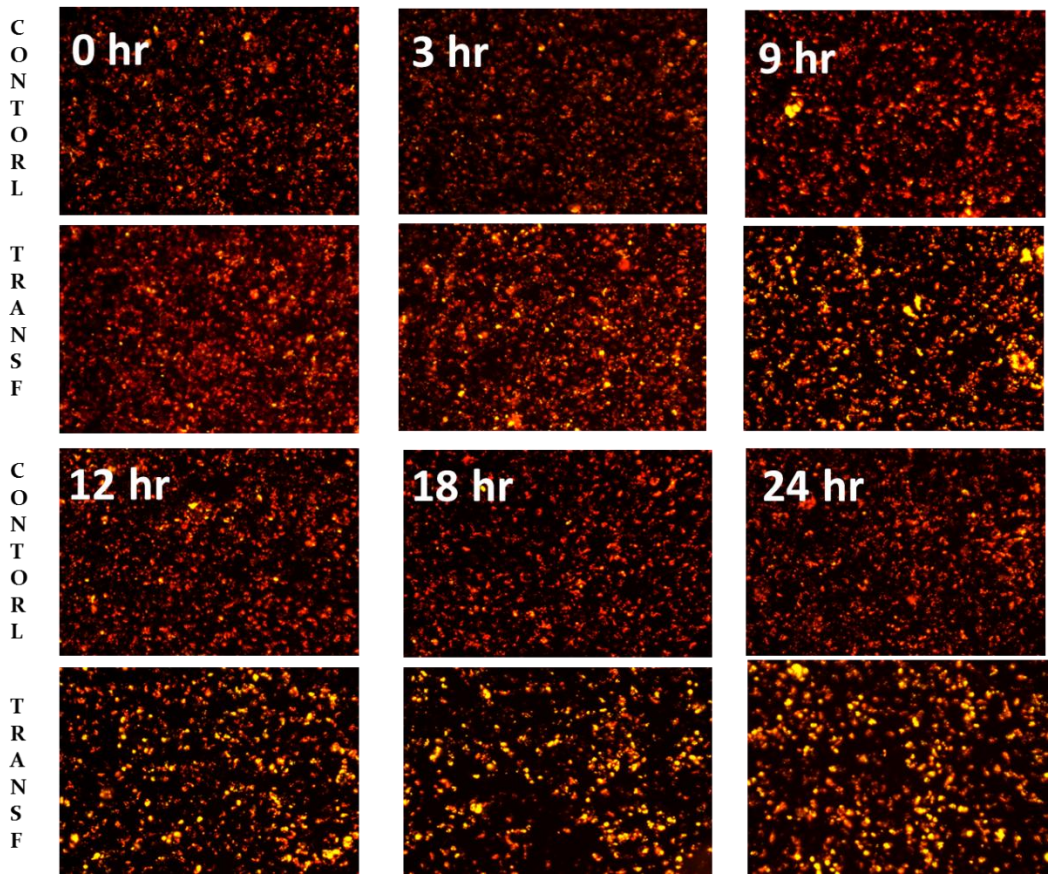

Figure 4. 6

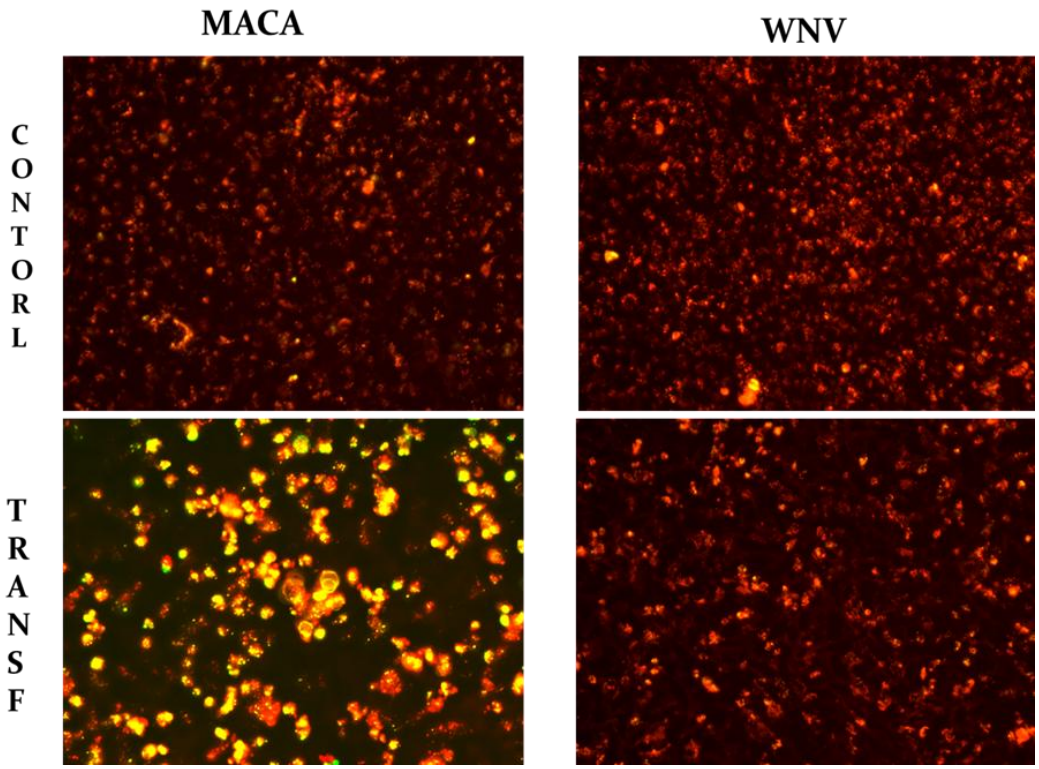

Figure 4. 7

A.

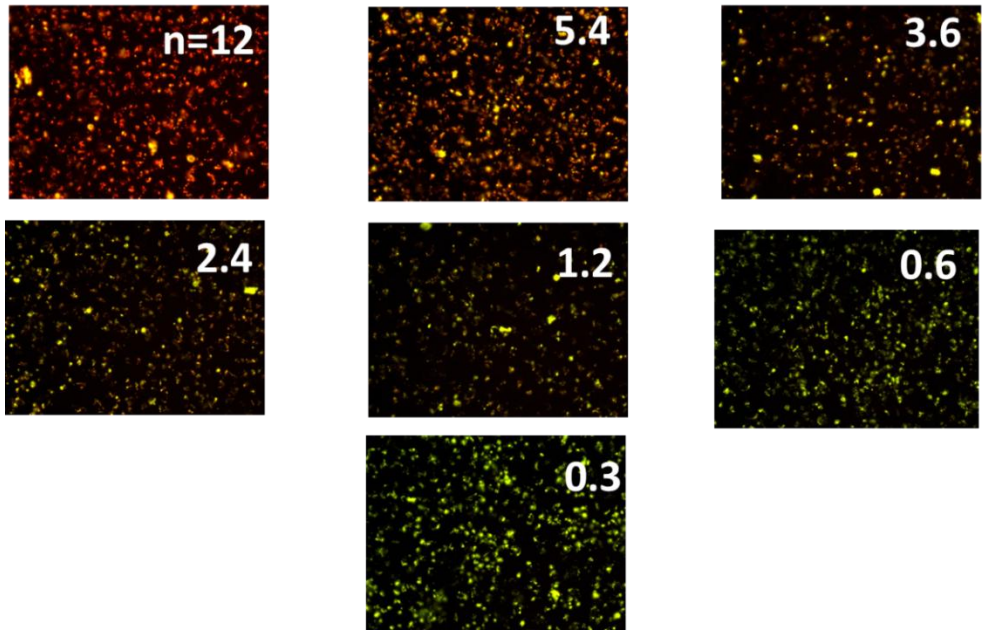
n=12
5.4
3.6
2.4
1.2
0.6
0.3

B.

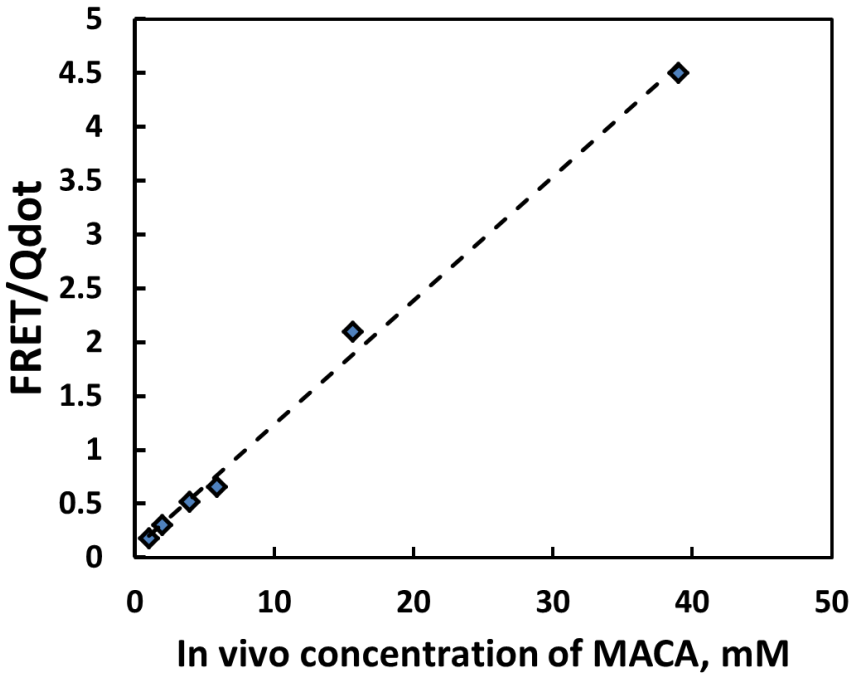
FRET/Qdot
0
0.5
1
1.5
2
2.5
3
3.5
4
4.5
5
0
10
20
30
40
50
In vivo concentration of MACA, mM

Figure 4. 8

A.

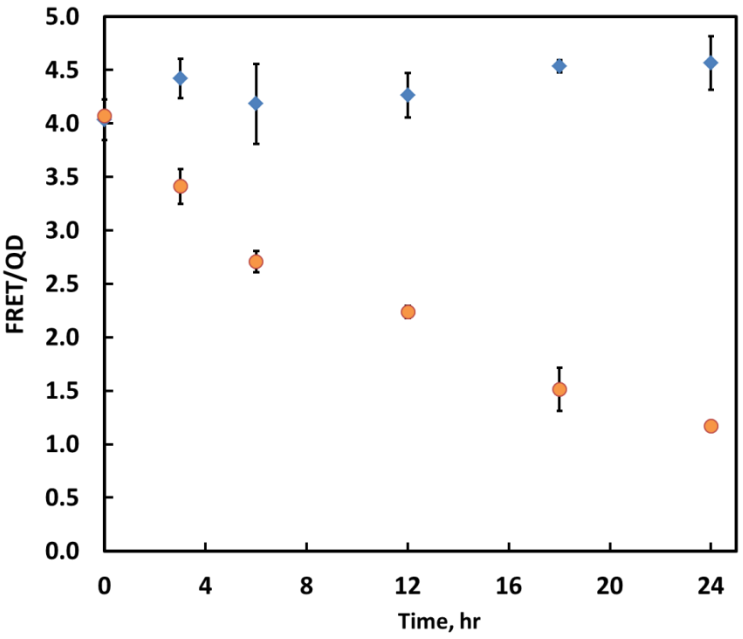
FRET/QD
5.0
4.5
4.0
3.5
3.0
2.5
2.0
1.5
1.0
0.5
0.0
0
4
8
12
16
20
24
Time, hr

B.

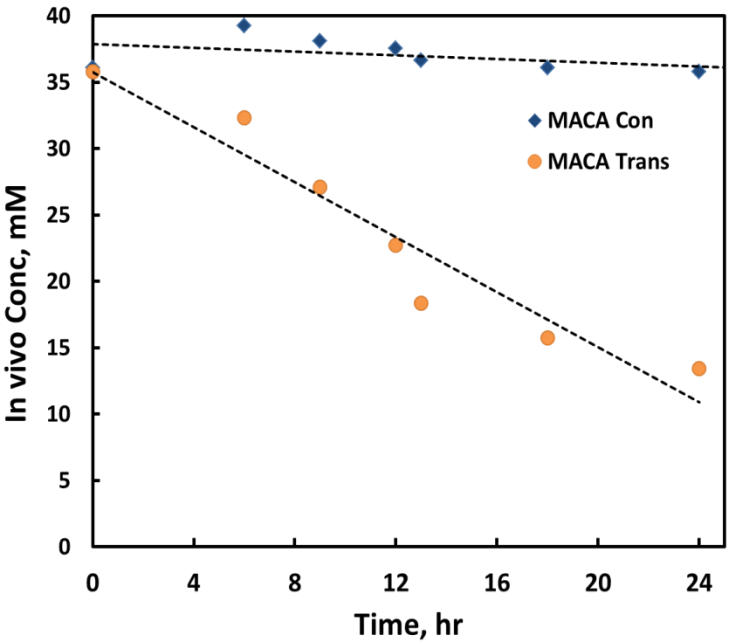
In vivo Conc, mM
40
35
30
25
20
15
10
5
0
0
4
8
12
16
20
24
Time, hr
MACA Con
MACA Trans

Figure 4. 9

A.

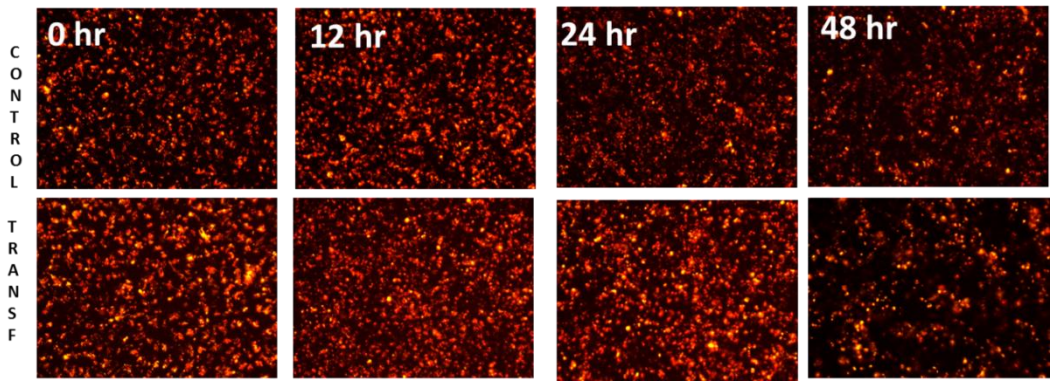
0 hr
12 hr
24 hr
48 hr
CONTROL
TRANSF

B.

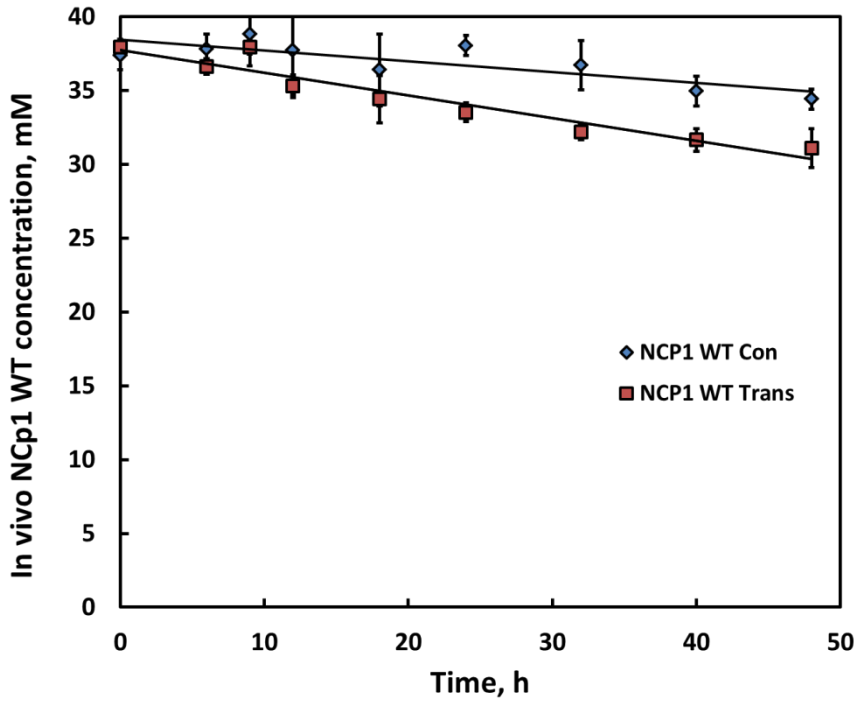
In vivo NCp1 WT concentration, mM
Time, h
NCP1 WT Con
NCP1 WT Trans
0
5
10
15
20
25
30
35
40
0
10
20
30
40
50

Figure 4. 10

A.

NCP1 Wild type (WT)	NCP1 Mutant(M2)
TERQAN↓FLGIWP	TERQVN↓FLGIWP

B.

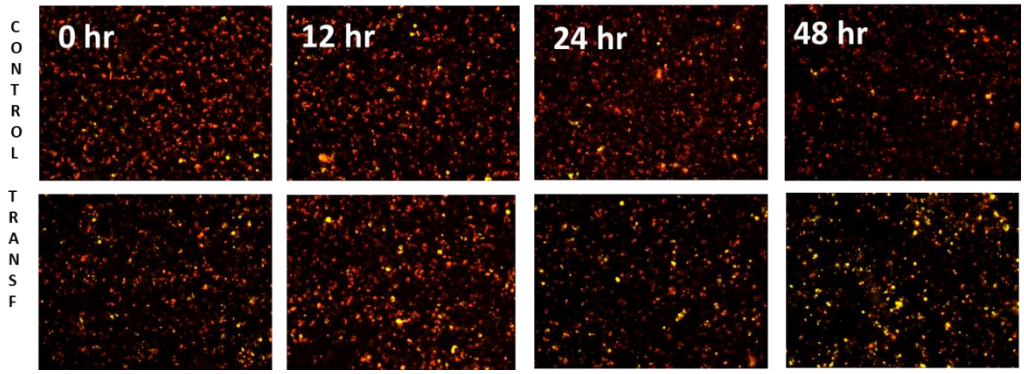

C.

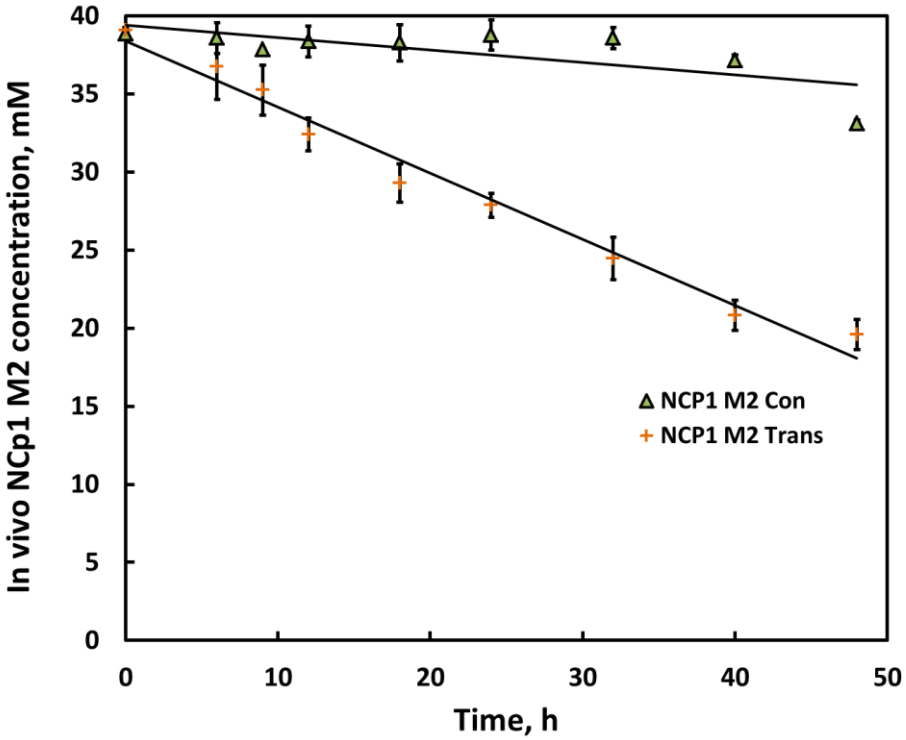

Figure 4. 11

A.

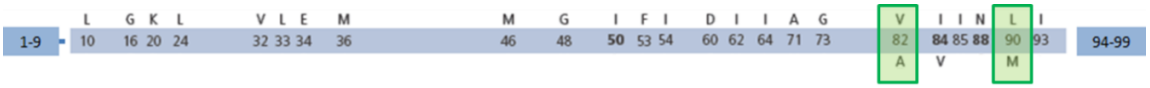

B.

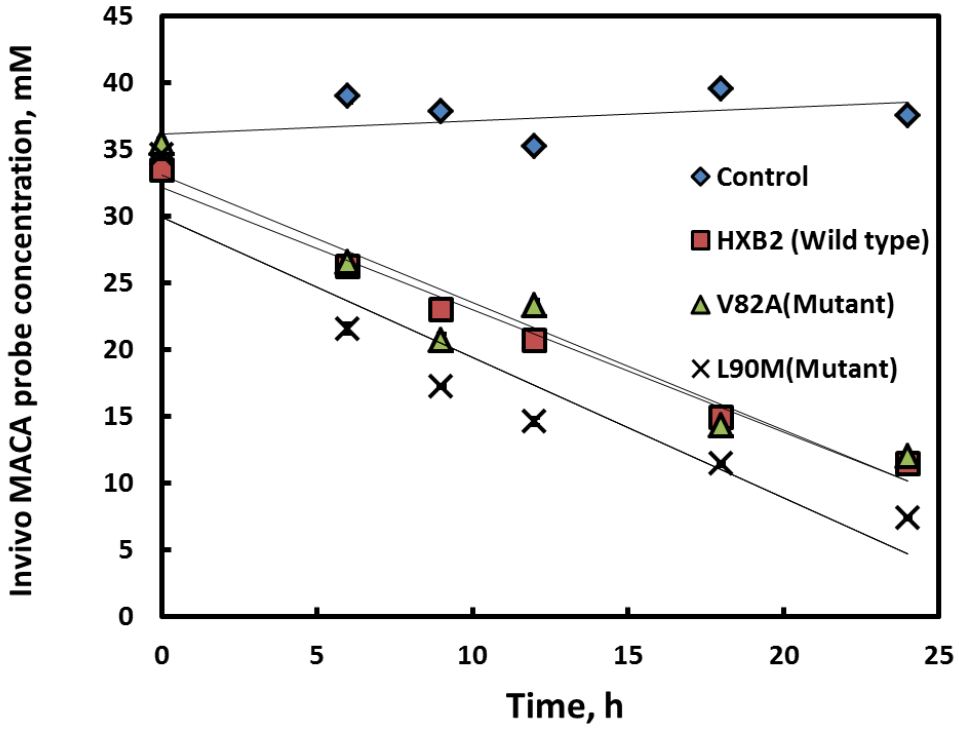

Figure 4. 12

A.

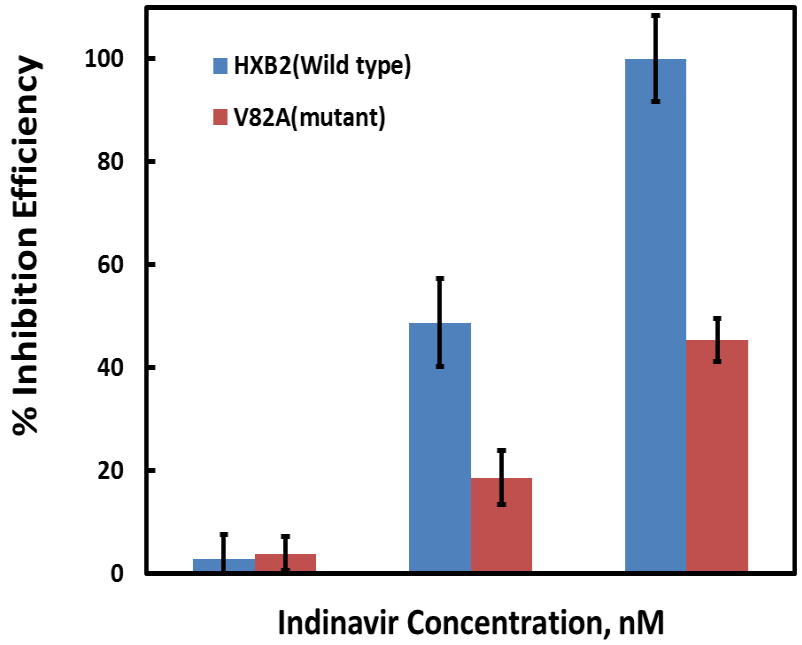

B.

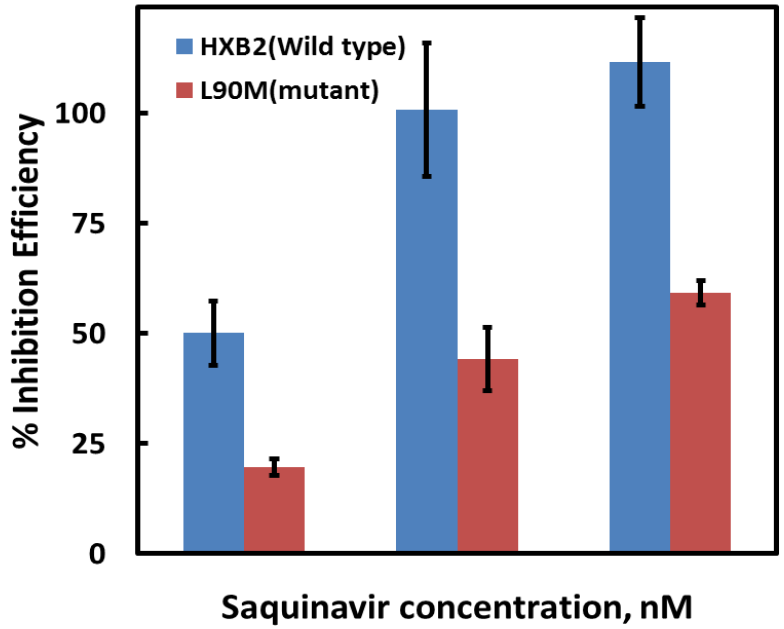

Table 4.1

	Reported IC_{50}	**Our Assay IC_{50}**		**Reported IC_{50}**	**Our Assay IC_{50}**
HXB2 (Wild type)	20 nM	10 nM	**HXB2 (Wild type)**	5 nM	5 nM
V82A(Mutant) + Indinavir	20 fold increase	>10 fold increase	**L90M(Mutant) + Saquinavir**	4-10 fold increase	10 fold increase

Conclusion

We have built novel diagnostic tools for detection of important targets affecting human health. Anthrax is a preferred bioweapon for antisocial elements to cause widespread damage to the society. The reason for this lies in the fact that it is hard to make an early detection of infection and failing to do so can lead to death. We have built a nano-biosensor that is highly sensitive and selective for detecting anthrax toxin. This sensor provides the advantage of simpler fabrication methodology, smaller size and can be reused, hence it can be mass produced at an affordable price for wide spread use. Using the same fabrication scheme but with a displacement mode of detection we were able to detect uncharged target molecule, glucose at picomolar levels. We have convincingly demonstrated that our biosensor platform is very versatile and can be adapted with little or no modification for detection of a variety of target molecules. We have developed an *in vivo* FRET based assay using a protein probe sensitive to HIV protease. HIV protease is shown to be an effective therapeutic target for blocking the infection. We can quantitatively assess the HIV protease activity against different cleavage sites using this cell based assay. This information can be used understand the protease interactions with different substrates and inhibitors. The flexibility of the design allows us to incorporate the drug resistance causing mutations in protease and capture the altered kinetics toward different substrates; thus gaining more understanding of the mechanism underlying the reduced sensitivity towards protease inhibitors. Our assay

can be a good choice for highly sought after cell based assay for screening new protease inhibitors. To screen for inhibitors that provide a high genetic barrier for the virus to delay drug resistance, we can mimic natural polymorphisms/mutations in the substrate and also protease mutations.

References

[1] M. Cinke, J. Li, B. Chen, A. Cassell, L. Delzeit, J. Han, and M. Meyyappan, "Pore structure of raw and purified HiPco single-walled carbon nanotubes," *Chemical Physics Letters*, vol. 365, no. 1–2, pp. 69–74, 2002.

[2] B. Q. Wei, R. Vajtai, and P. M. Ajayan, "Reliability and current carrying capacity of carbon nanotubes," *Applied Physics Letters*, vol. 79, no. 8, pp. 1172–1174, 2001.

[3] G. S. Bang, S. Cho, and B. G. Kim, "A novel electrochemical detection method for aptamer biosensors," *Biosensors & Bioelectronics*, vol. 21, no. 6, pp. 863–870, 2005.

[4] B. R. Baker, R. Y. Lai, M. S. Wood, E. H. Doctor, A. J. Heeger, and K. W. Plaxco, "An electronic, aptamer-based small-molecule sensor for the rapid, label-free detection of cocaine in adulterated samples and biological fluids," 2006.

[5] K. Ikebukuro, C. Kiyohara, and K. Sode, "Electrochemical detection of protein using a double aptamer sandwich," *Analytical Letters*, vol. 37, no. 14, pp. 2901–2909, 2004.

[6] R. Y. Lai, K. W. Plaxco, and A. J. Heeger, "Aptamer-based electrochemical detection of picomolar platelet-derived growth factor directly in blood serum," *Analytical Chemistry*, vol. 79, no. 1, pp. 229–233, 2007.

[7] H. M. So, K. Won, Y. H. Kim, B. K. Kim, B. H. Ryu, P. S. Na, H. Kim, and J. O. Lee, "Single-walled carbon nanotube biosensors using aptamers as molecular recognition elements," *Journal of the American Chemical Society*, vol. 127, no. 34, pp. 11906–11907, 2005.

[8] R. Kirby, E. J. Cho, B. Gehrke, T. Bayer, Y. S. Park, D. P. Neikirk, J. T. McDevitt, and A. D. Ellington, "Aptamer-based sensor arrays for the detection and quantitation of proteins," *Analytical Chemistry*, vol. 76, no. 14, pp. 4066–4075, 2004.

[9] C. K. Cote, C. A. Rossi, A. S. Kang, P. R. Morrow, J. S. Lee, and S. L. Welkos, "The detection of protective antigen (PA) associated with spores of Bacillus anthracis and the effects of anti-PA antibodies on spore germination and macrophage interactions," *Microbial Pathogenesis*, vol. 38, no. 5–6, pp. 209–225, 2005.

[10] M.-C. Lee, S. Kabilan, A. Hussain, X. Yang, J. Blyth, and C. R. Lowe, "Glucose-Sensitive Holographic Sensors for Monitoring Bacterial Growth," *Analytical Chemistry*, vol. 76, no. 19, pp. 5748–5755, 2004.

[11] X. Ge, L. Tolosa, and G. Rao, “Dual-Labeled Glucose Binding Protein for Ratiometric Measurements of Glucose,” *Analytical Chemistry*, vol. 76, no. 5, pp. 1403–1410, 2004.

[12] H. Zhang, Q. Zhao, S. Bhattacharya, A. A. Waheed, X. Tong, A. Hong, S. Heck, F. Curreli, M. Goger, D. Cowburn, E. O. Freed, and A. K. Debnath, “A cell-penetrating helical peptide as a potential HIV-1 inhibitor,” *J Mol Biol*, vol. 378, pp. 565–580, 2008.

[13] J. A. Jernigan, D. S. Stephens, D. A. Ashford, C. Omenaca, M. S. Topiel, M. Galbraith, M. Tapper, T. L. Fisk, S. Zaki, T. Popovic, R. F. Meyer, C. P. Quinn, S. A. Harper, S. K. Fridkin, J. J. Sejvar, C. W. Shepard, M. McConnell, J. Guarner, W. J. Shieh, J. M. Malecki, J. L. Gerberding, J. M. Hughes, and B. A. Perkins, “No Title,” *Emerging Infect. Dis.*, vol. 7, no. 6, p. 933, 2001.

[14] K. A. Bradley, J. Mogridge, M. Mourez, R. J. Collier, and J. A. T. Young, “Identification of the cellular receptor for anthrax toxin,” *Nature*, vol. 414, no. 6860, pp. 225–229, 2001.

[15] J. C. Milne, D. Furlong, P. C. Hanna, J. S. Wall, and R. J. Collier, “Anthrax Protective Antigen Forms Oligomers during Intoxication of mammalian Cells,” *Journal of Biological Chemistry*, vol. 269, no. 32, pp. 20607–20612, 1994.

[16] J. Mogridge, K. Cunningham, D. B. Lacy, M. Mourez, and R. J. Collier, “The lethal and edema factors of anthrax toxin bind only to oligomeric forms of the protective antigen,” *Proceedings of the National Academy of Sciences of the United States of America*, vol. 99, no. 10, pp. 7045–7048, 2002.

[17] S. H. Leppla, “Anthrax toxin edema factor : A bacterial adenylate cyclase that increases cyclic AMP concentrations in eukaryotic cells Biochemistry : Leppla,” vol. 79, no. May, pp. 3162–3166, 1982.

[18] N. S. Duesbery, C. P. Webb, S. H. Leppla, V. M. Gordon, K. R. Klimpel, T. D. Copeland, N. G. Ahn, M. K. Oskarsson, K. Fukasawa, K. D. Paull, and G. F. Vande Woude, “Proteolytic inactivation of MAP-kinase-kinase by anthrax lethal factor,” *Science*, vol. 280, no. 5364, pp. 734–737, 1998.

[19] K. M. Halverson, R. G. Panchal, T. L. Nguyen, R. Gussio, S. F. Little, M. Misakian, S. Bavari, and J. J. Kasianowicz, “Anthrax biosensor, protective antigen ion channel asymmetric blockade,” *Journal of Biological Chemistry*, vol. 280, no. 40, pp. 34056–34062, 2005.

[20] H.-Y. Park, H.-Y. Go, S. Kalme, R. S. Mane, S.-H. Han, and M.-Y. Yoon, “Protective Antigen Detection Using Horizontally Stacked Hexagonal ZnO Platelets,” *Analytical Chemistry*, vol. 81, no. 11, pp. 4280–4284, 2009.

[21] S. Sotiropoulou and N. A. Chaniotakis, “Carbon nanotube array-based biosensor,” *Analytical and Bioanalytical Chemistry*, vol. 375, no. 1, pp. 103–105, 2003.

[22] R. J. Chen, S. Bangsaruntip, K. A. Drouvalakis, N. W. S. Kam, M. Shim, Y. M. Li, W. Kim, P. J. Utz, and H. J. Dai, “Noncovalent functionalization of carbon nanotubes for highly specific electronic biosensors,” *Proceedings of the National Academy of Sciences of the United States of America*, vol. 100, no. 9, pp. 4984–4989, 2003.

[23] P. W. Barone and M. S. Strano, “Reversible control of carbon nanotube aggregation for a glucose affinity sensor,” *Angewandte Chemie-International Edition*, vol. 45, no. 48, pp. 8138–8141, 2006.

[24] H. Muguruma, S. Yoshida, M. Urata, K. Fujisawa, and Y. Matsui, “An amperometric biosensor for glucose based on a composite electrode of glucose dehydrogenase, carbon nanotubes, and plasma-polymerized thin films,” *Electrochemistry*, vol. 76, no. 8, pp. 545–548, 2008.

[25] J. S. Hwang, H. T. Kim, M. H. Son, J. H. Oh, S. W. Hwang, and D. Ahn, “Electronic transport properties of a single-wall carbon nanotube field effect transistor with deoxyribonucleic acid conjugation,” 2008, pp. 1115–1117.

[26] Y. Huang, H. G. Sudibya, D. Fu, R. Xue, X. Dong, L.-J. Li, and P. Chen, “Label-free detection of ATP release from living astrocytes with high temporal resolution using carbon nanotube network,” *Biosensors and Bioelectronics*, vol. 24, no. 8, pp. 2716–2720, 2009.

[27] D. W. Park, Y. H. Kim, B. S. Kim, H. M. So, K. Won, J. O. Lee, K. J. Kong, and H. Chang, “Detection of tumor markers using single-walled carbon nanotube field effect transistors,” *Journal of Nanoscience and Nanotechnology*, vol. 6, no. 11, pp. 3499–3502, 2006.

[28] S. N. Kim, J. F. Rusling, and F. Papadimitrakopoulos, “Carbon Nanotubes for Electronic and Electrochemical Detection of Biomolecules,” *Advanced Materials*, vol. 19, no. 20, pp. 3214–3228, 2007.

[29] S. Tang, M. Moayeri, Z. Chen, H. Harma, J. Zhao, H. Hu, R. H. Purcell, S. H. Leppla, and I. K. Hewlett, “Detection of Anthrax Toxin by an Ultrasensitive Immunoassay

Using Europium Nanoparticles," *Clinical and Vaccine Immunology*, vol. 16, no. 3, pp. 408–413, 2009.

[30] K. L. Ai, B. H. Zhang, and L. H. Lu, "Europium-Based Fluorescence Nanoparticle Sensor for Rapid and Ultrasensitive Detection of an Anthrax Biomarker," *Angewandte Chemie-International Edition*, vol. 48, no. 2, pp. 304–308, 2009.

[31] A. D. Ellington and J. W. Szostak, "In Vitro Selection of RNA molecules that bind specific ligands," *Nature*, vol. 346, no. 6287, pp. 818–822, 1990.

[32] C. Tuerk and L. Gold, "Systematic evolution of ligands by exponential enrichment - rna ligands to bacteriophage-t4 dna-polymerase," *Science*, vol. 249, no. 4968, pp. 505–510, 1990.

[33] S. D. Mendonsa and M. T. Bowser, "In vitro selection of aptamers with affinity for neuropeptide Y using capillary electrophoresis," *Journal of the American Chemical Society*, vol. 127, no. 26, pp. 9382–9383, 2005.

[34] S. D. Mendonsa and M. T. Bowser, "In vitro selection of high-affinity DNA ligands for human IgE using capillary electrophoresis," *Analytical Chemistry*, vol. 76, no. 18, pp. 5387–5392, 2004.

[35] K. Maehashi, T. Katsura, K. Kerman, Y. Takamura, K. Matsumoto, and E. Tamiya, "Label-free protein biosensor based on aptamer-modified carbon nanotube field-effect transistors," *Analytical Chemistry*, vol. 79, no. 2, pp. 782–787, 2007.

[36] P. C. Hanna, S. Kochi, and R. J. Collier, "Biochemical and physiological-changes induced by anthrax lethal toxin in j774 macrophage-like cells," *Molecular Biology of the Cell*, vol. 3, no. 11, pp. 1269–1277, 1992.

[37] J. W. Ezzell and T. G. Abshire, "Serum protease cleavage of bacillus-anthracis protective antigen," *Journal of General Microbiology*, vol. 138, pp. 543–549, 1992.

[38] R. Mabry, M. Rani, R. Geiger, G. B. Hubbard, R. Carrion, K. Brasky, J. L. Patterson, G. Georgiou, and B. L. Iverson, "Passive protection against anthrax by using a high-affinity antitoxin antibody fragment lacking an Fc region," *Infection and Immunity*, vol. 73, no. 12, pp. 8362–8368, 2005.

[39] R. G. Panchal, K. M. Halverson, W. Ribot, D. Lane, T. Kenny, T. G. Abshire, J. W. Ezzell, T. A. Hoover, B. Powell, S. Little, J. J. Kasianowicz, and S. Bavari, "Purified Bacillus anthracis lethal toxin complex formed in Vitro and during infection

exhibits functional and biological activity," *Journal of Biological Chemistry*, vol. 280, no. 11, pp. 10834–10839, 2005.

[40] S. Cload, "Novel Biosensors for detection of Biological warfare agents," *Report ID: DAAD19-02-C-0051*, 2002.

[41] J. Vivekananda and J. L. Kiel, "Anti-Francisella tularensis DNA aptamers detect tularemia antigen from different subspecies by Aptamer-Linked Immobilized Sorbent Assay," *Lab Invest*, vol. 86, no. 6, pp. 610–618, 2006.

[42] R. K. Mosing, S. D. Mendonsa, and M. T. Bowser, "Capillary electrophoresis-SELEX selection of aptamers with affinity for HIV-1 reverse transcriptase," *Analytical Chemistry*, vol. 77, no. 19, pp. 6107–6112, 2005.

[43] K. Yamamoto, S. Akita, and Y. Nakayama, "Orientation and purification of carbon nanotubes using ac electrophoresis," *Journal of Physics D-Applied Physics*, vol. 31, no. 8, pp. L34–L36, 1998.

[44] R. Mabry, K. Brasky, R. Geiger, R. Carrion, G. B. Hubbard, S. Leppla, J. L. Patterson, G. Georgiou, and B. L. Iverson, "Detection of anthrax toxin in the serum of animals infected with Bacillus anthracis by using engineered immunoassays," *Clinical and Vaccine Immunology*, vol. 13, no. 6, pp. 671–677, 2006.

[45] C. W. Wang, C. Y. Pan, H. C. Wu, P. Y. Shih, C. C. Tsai, K. T. Liao, L. L. Lu, W. H. Hsieh, C. D. Chen, and Y. T. Chen, "In situ detection of chromogranin a released from living neurons with a single-walled carbon-nanotube field-effect transistor," *Small*, vol. 3, no. 8, pp. 1350–1355, 2007.

[46] R. J. Chen, H. C. Choi, S. Bangsaruntip, E. Yenilmez, X. W. Tang, Q. Wang, Y. L. Chang, and H. J. Dai, "An investigation of the mechanisms of electronic sensing of protein adsorption on carbon nanotube devices," *Journal of the American Chemical Society*, vol. 126, no. 5, pp. 1563–1568, 2004.

[47] L. N. Cella, P. Sanchez, W. Zhong, N. V Myung, W. Chen, and A. Mulchandani, "Nano Aptasensor for Protective Antigen Toxin of Anthrax," vol. 82, no. 5, pp. 2042–2047, 2010.

[48] J. Oh, S. Yoo, Y. W. Chang, K. Lim, and K.-H. Yoo, "Carbon nanotube-based biosensor for detection hepatitis B," *Current Applied Physics*, vol. 9, no. 4, pp. e229–e231, Jul. 2009.

[49] H. M. So, D. W. Park, E. K. Jeon, Y. H. Kim, B. S. Kim, C. K. Lee, S. Y. Choi, S. C. Kim, H. Chang, and J. O. Lee, “Detection and titer estimation of Escherichia coli using aptamer-functionalized single-walled carbon-nanotube field-effect transistors,” *Small*, vol. 4, no. 2, pp. 197–201, 2008.

[50] R. A. Villamizar, A. Maroto, and F. X. Rius, “Improved detection of Candida albicans with carbon nanotube field-effect transistors,” *Sensors and Actuators B-Chemical*, vol. 136, no. 2, pp. 451–457, 2009.

[51] T. Dastagir, E. S. Forzani, R. Zhang, I. Amlani, L. a Nagahara, R. Tsui, and N. Tao, “Electrical detection of hepatitis C virus RNA on single wall carbon nanotube-field effect transistors.,” *The Analyst*, vol. 132, no. 8, pp. 738–40, Aug. 2007.

[52] X. Tang, S. Bansaruntip, N. Nakayama, E. Yenilmez, Y.-L. Chang, and Q. Wang, “Carbon nanotube DNA sensor and sensing mechanism.,” *Nano letters*, vol. 6, no. 8, pp. 1632–6, Aug. 2006.

[53] X. Dong, C. M. Lau, A. Lohani, S. G. Mhaisalkar, J. Kasim, Z. Shen, X. Ho, J. a. Rogers, and L.-J. Li, “Electrical Detection of Femtomolar DNA via Gold-Nanoparticle Enhancement in Carbon-Nanotube-Network Field-Effect Transistors,” *Advanced Materials*, vol. 20, no. 12, pp. 2389–2393, Jun. 2008.

[54] N. Shao, E. Wickstrom, and B. Panchapakesan, “Nanotube-antibody biosensor arrays for the detection of circulating breast cancer cells,” *Nanotechnology*, vol. 19, no. 46, 2008.

[55] S. H. Sheikh and A. Mulchandani, “Continuous-flow fluoro-immunosensor for paclitaxel measurement,” *Biosensors & Bioelectronics*, vol. 16, no. 9–12, pp. 647–652, 2001.

[56] U. Narang, P. R. Gauger, and F. S. Ligler, “A displacement flow immunosensor for explosive detection using microcapillaries,” *Analytical Chemistry*, vol. 69, no. 14, pp. 2779–2785, 1997.

[57] F. Vianello, L. Signor, A. Pizzariello, M. L. Di Paolo, M. Scarpa, B. Hock, T. Giersch, and A. Rigo, “Continuous flow immunosensor for atrazine detection,” *Biosensors & Bioelectronics*, vol. 13, no. 1, pp. 45–53, 1998.

[58] K. Kronkvist, U. LÃ¶vgren, J. Svenson, L. E. Edholm, and G. Johansson, “Competitive flow injection enzyme immunoassay for steroids using a post-column reaction technique,” *Journal of Immunological Methods*, vol. 200, no. 1–2, pp. 145–153, 1997.

[59] W. A. Kaptein, J. J. Zwaagstra, K. Venema, M. H. J. Ruiters, and J. Korf, “Analysis of cortisol with a flow displacement immunoassay,” *Sensors and Actuators, B: Chemical*, vol. 45, no. 1, pp. 63–69, 1997.

[60] G. A. Wemhoff, S. Y. Rabbany, A. W. Kusterbeck, R. A. Ogert, R. Bredehorst, and F. S. Ligler, “Kinetics of antibody binding at solid-liquid interfaces in flow,” *Journal of Immunological Methods*, vol. 156, no. 2, pp. 223–230, 1992.

[61] J. S. Schultz, “Optical sensor of plasma constituents,” .

[62] S. Mansouri and J. S. Schultz, “A miniature optical glucose sensor based on affinity binding,” *Bio-Technology*, vol. 2, no. 10, pp. 885–890, 1984.

[63] R. Ballerstadt, C. Evans, A. Gowda, and R. McNichols, “In vivo performance evaluation of a transdermal near-infrared fluorescence resonance energy transfer affinity sensor for continuous glucose monitoring,” *Diabetes Technology & Therapeutics*, vol. 8, no. 3, pp. 296–311, Jun. 2006.

[64] S. H. Gordon and J. G. Irwin, “Ultraviolet Difference Spectral Studies on Concanavalin A,” *European Journal of Biochemistry*, vol. 16, no. 3, pp. 549–556, 1970.

[65] J. B. Sumner and S. F. Howell, “Inactivation of Hemagglutinin,” pp. 583–588.

[66] G. Gruner, “Carbon nanotube transistors for biosensing applications,” *Analytical and Bioanalytical Chemistry*, vol. 384, no. 2, pp. 322–335, 2006.

[67] A. Star, J. C. P. Gabriel, K. Bradley, and G. Gruner, “Electronic detection of specific protein binding using nanotube FET devices,” *Nano Letters*, vol. 3, no. 4, pp. 459–463, 2003.

[68] I. Heller, A. M. Janssens, J. Männik, E. D. Minot, S. G. Lemay, and C. Dekker, “Identifying the mechanism of biosensing with carbon nanotube transistors.,” *Nano letters*, vol. 8, no. 2, pp. 591–5, Feb. 2008.

[69] T. Bo, C. Lihua, X. Kehua, Z. Linhai, G. Jiechao, L. Qingling, and Y. Lijuan, “A New Nanobiosensor for Glucose with High Sensitivity and Selectivity in Serum Based on Fluorescence Resonance Energy Transfer (FRET) between CdTe Quantum Dots and Au Nanoparticles,” *Chemistry - A European Journal*, vol. 14, no. 12, pp. 3637–3644, 2008.

[70] M. Yamaguchi, Y. Kano, and M. Mitsumori, “Noninvasive procedure for monitoring blood glucose using a saliva analyzing system,” *Transactions of the Institute of Electrical Engineers of Japan, Part E*, vol. 118-E, no. 12, pp. 621–626, 1998.

[71] M. Miyashita, N. Ito, S. Ikeda, T. Murayama, K. Oguma, and J. Kimura, “Development of urine glucose meter based on micro-planer amperometric biosensor and its clinical application for self-monitoring of urine glucose.,” *Biosensors & bioelectronics*, vol. 24, no. 5, pp. 1336–40, Jan. 2009.

[72] T. M. O’Connell, F. Ardeshirpour, S. a. Asher, J. H. Winnike, X. Yin, J. George, D. C. Guttridge, W. He, A. Wysong, M. S. Willis, and M. E. Couch, “Metabolomic analysis of cancer cachexia reveals distinct lipid and glucose alterations,” *Metabolomics*, vol. 4, no. 3, pp. 216–225, Jul. 2008.

[73] M. Fehr, H. Takanaga, D. W. Ehrhardt, and B. Frommer, “Evidence for High-Capacity Bidirectional Glucose Transport across the Endoplasmic Reticulum Membrane by Genetically Encoded Fluorescence Resonance Energy Transfer Nanosensors Evidence for High-Capacity Bidirectional Glucose Transport across the Endoplasmi,” *Molecular and Cellular Biology*, vol. 25, no. 24, pp. 11102–11112, 2005.

[74] M. a Sommerfelt, “Retrovirus receptors.,” *The Journal of general virology*, vol. 80 (Pt 12, pp. 3049–64, Dec. 1999.

[75] L. Menéndez-Arias, “Targeting HIV: antiretroviral therapy and development of drug resistance.,” *Trends in pharmacological sciences*, vol. 23, no. 8, pp. 381–8, Aug. 2002.

[76] S. G. Sarafianos, B. Marchand, K. Das, D. M. Himmel, M. a Parniak, S. H. Hughes, and E. Arnold, “Structure and function of HIV-1 reverse transcriptase: molecular mechanisms of polymerization and inhibition.,” *Journal of molecular biology*, vol. 385, no. 3, pp. 693–713, Jan. 2009.

[77] T. W. Chun, L. Carruth, D. Finzi, X. F. Shen, J. A. DiGiuseppe, H. Taylor, M. Hermankova, K. Chadwick, J. Margolick, T. C. Quinn, Y. H. Kuo, R. Brookmeyer, M. A. Zeiger, P. BarditchCrovo, and R. F. Siliciano, “Quantification of latent tissue reservoirs and total body viral load in HIV-1 Infection,” *NATURE*, vol. 387, no. 6629, pp. 183–188, May 1997.

[78] M. A. Navia, P. M. D. Fitzgerald, B. M. McKeever, C. T. Leu, J. C. Heimbach, W. K. Herber, I. S. Sigal, P. L. Darke, and J. P. Springer, “3-Dimensional structure of

aspartyl protease from human immunodeficiency virus hiv-1," *Nature*, vol. 337, no. 6208, pp. 615–620, Feb. 1989.

[79] J. C. Craig, I. B. Duncan, D. Hockley, C. Grief, N. A. Roberts, and J. S. Mills, "Antiviral properties of Ro 31-8959, an inhibitor of human immunodeficiency virus (HIV) proteinase," *Antiviral Res*, vol. 16, pp. 295–305, 1991.

[80] Y. Koh, S. Matsumi, D. Das, M. Amano, D. A. Davis, J. Li, S. Leschenko, A. Baldridge, T. Shioda, R. Yarchoan, A. K. Ghosh, and H. Mitsuya, "Potent inhibition of HIV-1 replication by novel non-peptidyl small molecule inhibitors of protease dimerization," *J Biol Chem*, vol. 282, pp. 28709–28720, 2007.

[81] M. Prabu-Jeyabalan, E. Nalivaika, and C. A. Schiffer, "Substrate shape determines specificity of recognition for HIV-1 protease: analysis of crystal structures of six substrate complexes," *Structure*, vol. 10, pp. 369–381, 2002.

[82] E. Dam, R. Quercia, B. Glass, D. Descamps, O. Launay, X. Duval, H. G. Krausslich, A. J. Hance, and F. Clavel, "Gag mutations strongly contribute to HIV-1 resistance to protease inhibitors in highly drug-experienced patients besides compensating for fitness loss," *PLoS Pathog*, vol. 5, p. e1000345, 2009.

[83] L. Doyon, G. Croteau, D. Thibeault, F. Poulin, L. Pilote, and D. Lamarre, "Second locus involved in human immunodeficiency virus type 1 resistance to protease inhibitors," *J Virol*, vol. 70, pp. 3763–3769, 1996.

[84] M. Nijhuis, N. M. van Maarseveen, S. Lastere, P. Schipper, E. Coakley, B. Glass, M. Rovenska, D. de Jong, C. Chappey, I. W. Goedegebuure, G. Heilek-Snyder, D. Dulude, N. Cammack, L. Brakier-Gingras, J. Konvalinka, N. Parkin, H. G. Krausslich, F. Brun-Vezinet, and C. A. Boucher, "A novel substrate-based HIV-1 protease inhibitor drug resistance mechanism," *PLoS Med*, vol. 4, p. e36, 2007.

[85] C. Roh, H.-Y. Lee, S.-E. Kim, and S.-K. Jo, "A highly sensitive and selective viral protein detection method based on RNA oligonucleotide nanoparticle," *International journal of nanomedicine*, vol. 5, pp. 323–329, 2010.

[86] P. Biswas, L. N. Cella, S. H. Kang, A. Mulchandani, M. V Yates, and W. Chen, "A quantum-dot based protein module for in vivo monitoring of protease activity through fluorescence resonance energy transfer," *Chem. Commun.*, vol. 47, no. 18, pp. 5259–5261, 2011.

[87] D. W. Urry, "Physical Chemistry of Biological Free Energy Transduction As Demonstrated by Elastic," vol. 5647, no. 97, pp. 11007–11028, 1997.

[88] H. Brooks, B. Lebleu, and E. Vivès, “Tat peptide-mediated cellular delivery: back to basics.,” *Advanced drug delivery reviews*, vol. 57, no. 4, pp. 559–77, Feb. 2005.

[89] S.-W. Lu, J.-W. Hu, B. R. Liu, C.-Y. Lee, J.-F. Li, J.-C. Chou, and H.-J. Lee, “Arginine-rich intracellular delivery peptides synchronously deliver covalently and noncovalently linked proteins into plant cells.,” *Journal of agricultural and food chemistry*, vol. 58, no. 4, pp. 2288–94, Feb. 2010.

[90] J.-C. Lee, M.-C. Yu, T.-W. Lien, C.-F. Chang, and J. T. Hsu, “High-throughput cell-based screening for hepatitis C virus NS3/4A protease inhibitors.,” *Assay and drug development technologies*, vol. 3, no. 4, pp. 385–92, Aug. 2005.

[91] Y. Hwang, W. Chen, and M. V Yates, “Use of Fluorescence Resonance Energy Transfer for Rapid Detection of Enteroviral Infection In Vivo Use of Fluorescence Resonance Energy Transfer for Rapid Detection of Enteroviral Infection In Vivo †,” *Applied and Environmental Microbiology*, vol. 72, no. 5, pp. 3710–3715, 2006.

[92] B. J. Hilton and R. Wolkowicz, “An assay to monitor HIV-1 protease activity for the identification of novel inhibitors in T-cells.,” *PloS one*, vol. 5, no. 6, p. e10940, Jan. 2010.

[93] K. Lindsten and A. Tat, “Cell-Based Fluorescence Assay for Human Immunodeficiency Virus Type 1 Protease Activity,” vol. 45, no. 9, pp. 2616–2622, 2001.

[94] M. J. Buzon, I. Erkizia, C. Pou, G. Minuesa, M. C. Puertas, A. Esteve, A. Castello, J. R. Santos, J. G. Prado, N. Izquierdo-Useros, T. Pattery, M. Van Houtte, L. Carrasco, B. Clotet, L. Ruiz, and J. Martinez-Picado, “A non-infectious cell-based phenotypic assay for the assessment of HIV-1 susceptibility to protease inhibitors.,” *The Journal of antimicrobial chemotherapy*, vol. 67, no. 1, pp. 32–8, Jan. 2012.

[95] J.-Y. Kim, A. Mulchandani, and W. Chen, “Temperature-triggered purification of antibodies.,” *Biotechnology and bioengineering*, vol. 90, no. 3, pp. 373–9, May 2005.

[96] A. R. Clapp, E. R. Goldman, and H. Mattoussi, “Capping of CdSe-ZnS quantum dots with DHLA and subsequent conjugation with proteins.,” *Nature protocols*, vol. 1, no. 3, pp. 1258–66, Jan. 2006.

[97] R. I. Connor, B. K. Chen, S. Choe, and N. R. Landau, “VPR is required for efficient replication of human-immunodeficiency-virus type-1 in mononuclear phagocytes,” *Virology*, vol. 206, no. 2, pp. 935–944, Feb. 1995.

[98] J. He, S. Choe, R. Walker, P. D. I. Marzio, and D. O. Morgan, “Human Immunodeficiency Virus Type 1 Viral Protein R (Vpr) Arrests Cells in the G 2 Phase of the Cell Cycle by Inhibiting p34 cdc2 Activity,” vol. 69, no. 11, pp. 6705–6711, 1995.

[99] J. R. Lakowicz, *Principles of Fluroscence Spectroscopy*, 2 nd. New York: Kluwer Academic, 1999.

[100] A. R. Clapp, I. L. Medintz, J. M. Mauro, B. R. Fisher, M. G. Bawendi, and H. Mattoussi, “Fluorescence Resonance Energy Transfer Between Quantum Dot Donors and Dye-Labeled Protein Acceptors ¨ rster resonance energy transfer,” no. 7, pp. 301–310, 2004.

[101] Y. S. Cheng, F. H. Yin, S. Foundling, D. Blomstrom, and C. a Kettner, “Stability and activity of human immunodeficiency virus protease: comparison of the natural dimer with a homologous, single-chain tethered dimer.,” *Proceedings of the National Academy of Sciences of the United States of America*, vol. 87, no. 24, pp. 9660–4, Dec. 1990.

[102] J. Tözsér, I. Bláha, T. D. Copeland, E. M. Wondrak, and S. Oroszlan, “Comparison of the HIV-1 and HIV-2 proteinases using oligopeptide substrates representing cleavage sites in Gag and Gag-Pol polyproteins.,” *FEBS letters*, vol. 281, no. 1–2, pp. 77–80, Apr. 1991.

[103] A. Feher, I. T. Weber, P. Bagossi, P. Boross, B. Mahalingam, J. M. Louis, T. D. Copeland, I. Y. Torshin, R. W. Harrison, and J. Tozser, “Effect of sequence polymorphism and drug resistance on two HIV-1 Gag processing sites,” *Eur J Biochem*, vol. 269, pp. 4114–4120, 2002.

[104] U. Landesbibliothek, “Fundamentals of Enzyme Kinetics by Athel Cornish-Bowden.”

[105] A. Fehér, I. T. Weber, P. Bagossi, P. Boross, B. Mahalingam, J. M. Louis, T. D. Copeland, I. Y. Torshin, R. W. Harrison, and J. Tözsér, “Effect of sequence polymorphism and drug resistance on two HIV-1 Gag processing sites,” *European Journal of Biochemistry*, vol. 269, no. 16, pp. 4114–4120, Aug. 2002.

[106] B. Maschera, G. Darby, G. Palu, L. L. Wright, M. Tisdale, R. Myers, E. D. Blair, and E. S. Furfine, “Mutations in the viral protease that confer resistance to saquinavir increase the dissociation rate constant of the protease-saquinavir complex,” vol. 271, no. 52, pp. 33231–33235, 1996.

[107] E. M. Wondrack, J. M. Louis, H. Derocquigny, J. C. Chermann, and B. P. Roques, “The gag precursor contains a specific HIV-1 protease cleavage site between the NC (P7) and p1 proteins,” *FEBS Letters*, vol. 333, no. 1–2, pp. 21–24, Oct. 1993.

[108] F. Bally, R. Martinez, S. Peters, P. Sudre, and A. Telenti, “Polymorphism of HIV type 1 gag p7/p1 and p1/p6 cleavage sites: clinical significance and implications for resistance to protease inhibitors,” *AIDS Res Hum Retroviruses*, vol. 16, pp. 1209–1213, 2000.

[109] A. Molla, M. Korneyeva, Q. Gao, S. Vasavanonda, P. J. Schipper, H. M. Mo, M. Markowitz, T. Chernyavskiy, P. Niu, N. Lyons, A. Hsu, G. R. Granneman, D. D. Ho, C. A. B. Boucher, J. M. Leonard, D. W. Norbeck, and D. J. Kempf, “Ordered accumulation of mutations in HIV protease confers resistance to ritonavir,” *NATURE MEDICINE*, vol. 2, no. 7, pp. 760–766, Jul. 1996.

[110] H. C. F. Côté, Z. L. Brumme, P. Richard, and P. R. Harrigan, “Human Immunodeficiency Virus Type 1 Protease Cleavage Site Mutations Associated with Protease Inhibitor Cross-Resistance Selected by Indinavir , Ritonavir , and / or Saquinavir Human Immunodeficiency Virus Type 1 Protease Cleavage Site Mutations Associate,” 2001.

[111] Y. M. Zhang, H. Imamichi, T. Imamichi, H. C. Lane, J. Falloon, M. B. Vasudevachari, and N. P. Salzman, “Drug resistance during indinavir therapy is caused by mutations in the protease gene and in its Gag substrate cleavage sites.,” *Journal of virology*, vol. 71, no. 9, pp. 6662–70, Sep. 1997.

[112] M. Kolli, E. Stawiski, C. Chappey, and C. a Schiffer, “Human immunodeficiency virus type 1 protease-correlated cleavage site mutations enhance inhibitor resistance.,” *Journal of virology*, vol. 83, no. 21, pp. 11027–42, Nov. 2009.